Open Access

*Recent Progress in Materials*

LIDSEN Publishing Inc.

Review

# Self-Consistent Theory of Screening and Transport in Narrow, Translation-Invariant Hall Bars under the Conditions of the Integer Quantum-Hall-Effect

Rolf R. Gerhardts *

Max-Planck-Institut für Festkörperforschung, Heisenbergstrasse 1, D-70569 Stuttgart, Germany; E-Mail: R.Gerhardts@fkf.mpg.de

* **Correspondence:** Rolf R. Gerhardts; E-Mail: R.Gerhardts@fkf.mpg.de

**Academic Editor:** Sotirios Baskoutas

**Special Issue**: Quantum Confinement Effects in Nano Material

*Recent Progress in Materials*
2020, volume 2, issue 1
doi:10.21926/rpm.2001007

**Received:** November 11, 2019
**Accepted:** February 10, 2020
**Published:** March 17, 2020

**Abstract**

We summarize and discuss a self-consistent screening and magneto-transport theory, developed to understand the results of scanning-force-microscope experiments on the current distribution in a two-dimensional electron system (2DES), located in a narrow Hall bar under the conditions of the integer quantum Hall effect (IQHE) and its breakdown. The theory explains why, at low temperatures, at certain intervals of the applied perpendicular magnetic field, the current density is confined to "incompressible stripes" (ISs), in which a fixed number of Landau levels is occupied, and the longitudinal and Hall resistivity assume quantized values. The theory also explains, how the position and shape of these ISs depend on magnetic field and temperature, and why the confinement of the current density on these ISs leads to precisely quantized values of the macroscopic longitudinal and Hall resistance. The theory, which leads, at high temperatures, to the well known Drude results for current density and resistance, shows that the IQHE is a consequence of the peculiar screening properties of a 2DES in a strong magnetic field at low temperatures, and that it can be understood without assumptions about special localization effects.

## 1. Introduction

The “Quantum Hall Effect” (QHE), discovered 1980 by K. von Klitzing [1], who was honored by the Nobel Price in 1985, presents a unique possibility to reproduce, in different materials, the electrical resistance $R_K = h/e^2 = 25812.80745\,\Omega$ (von-Klitzing constant) with extremely high accuracy, and is nowadays used as one basic constant for the definition of the international system of physical units [2, 3]. The QHE was detected on a quasi-two-dimensional electron system (2DES) in a Si-MOSFET (silicon-based metal-oxide-semiconductor field-effect-transistor) in a strong perpendicular magnetic field at low temperatures. While changing the electron density with a suitable gate voltage, the longitudinal resistance $R_{\mathrm{long}}$ showed the expected Shubnikov–de Haas oscillations, but, in certain density intervals of finite width, $R_{\mathrm{long}}$ vanished, whereas in these intervals the Hall resistance was constant with values $R_{\mathrm{Hall}} = h/(ie^2)$ with an integer value $i = 1, 2, 3, \ldots$ Later this effect was also found in other materials, e.g., in GaAs/(AlGa)As heterostructures, and the quantized values $R_{\mathrm{long}} = 0$ and $R_{\mathrm{Hall}} = h/(ie^2)$ could be measured with even higher accuracy. Nowadays this effect is usually known as the "Integer QHE" (IQHE), because in very high magnetic fields and at very low temperatures, a similar “fractional QHE” has been detected, where $i$ is replaced by the ratio of two relatively small integers [4]. Under the conditions of the IQHE the resistance of a real 2DES appears as the resistance of an ideal electron gas with an integer value of the Landau level filling factor.

In spite of its practical use, the theoretical understanding of the IQHE still raises some open questions. Early attempts tried to understand the IQHE as a single-particle effect and neglected the Coulomb interaction between the conduction electrons as irrelevant. In the absence of a magnetic field, the conduction electrons need quasi-elastic scattering, in order to respond to a constant source-drain voltage with a stationary current. This implies that, at low temperatures, only the states with energy eigenvalues near the Fermi energy can be relevant for the current. In a strong magnetic field $B$, the energy spectrum shows Landau quantization and, near the sample edges, the Landau energies increase. The resulting Landau bands cross the Fermi energy and lead to a decrease in the electron density toward the edges. The increase in the energy band toward an edge produces an electric field perpendicular to the edge and thus a Hall current parallel to the edge. These edge-currents, which have opposite directions at opposite edges of the sample, and can be modified by an applied source-drain voltage, have been considered as responsible for the current transport through the sample.

In order to understand, why at constant electron density, the values of longitudinal and Hall resistance are constant in certain $B$-intervals of finite width, i.e., in the "quantum Hall plateaus" (QHPs), it was assumed that certain electron states are localized and do not contribute to the current. There are a large number of theoretical papers, presenting different results concerning the distribution of an applied source-drain current (ASDC) in the sample (see [5-8] and references therein). Some experiments seem to indicate the transport through edge-states, but not all [9]. Unfortunately, up to now, there exist no experiments, which can measure the local current distribution in macroscopic samples, for which the assumption of constant electron density may be a good approximation.

This is different in microscopically narrow samples (width $W \gtrsim 10\,\mu$m), which contain a two-dimensional electron system (2DES) that is not too far below the surface. For these samples, scanning-force-microscopy experiments allow measuring the local distribution of the Hall potential across the sample under the conditions of the IQHE, and to deduce from these results the local distribution of the ASDC [10-13]. These experiments clearly showed that under the conditions of the IQHE the ASDC is carried by stripes, which change the position and width as a function of the applied magnetic field in the manner, as the "incompressible stripes" (ISs) do, which were predicted by Chklovskii *et al.* [14, 15]. These ISs occur as a consequence of the peculiar screening properties of an inhomogeneous 2DES at zero temperature in a high magnetic field, and are characterized by integer values of the local Landau-level filling-factor.

The peculiar screening properties of a 2DES in a perpendicular, high magnetic field $B$ at low temperature $T$ result from the Landau quantization and the macroscopic degeneracy of the discrete Landau energy levels. For a *homogeneous* 2DES (with density $n_{el}$ at chemical potential $\mu$), this leads to a thermodynamic density of states (TDOS) $dn_{el}/d\mu$, which exhibits strong oscillations as a function of $B$. If $\mu$ coincides (within $k_BT$) with a Landau level (LL), the TDOS is very large, the screening ability of the 2DES is very good, and (sufficiently week) potential fluctuations are nearly perfectly screened by a suitable rearrangement of the 2D electron density. But if $\mu$ is deep in a Landau gap, separated by more than $k_BT$ from the adjacent LLs, there exist no states with energy near $\mu$, the TDOS is very small, potential fluctuation cannot be screened, and the electron density is determined by the integer number of completely filled LLs.

In an *inhomogeneous*, laterally confined 2DES, where confinement potential and electron density vary so strongly that in different parts of the system a different number of LLs is occupied, both screening situations occur. In "compressible" regions with position-dependent electron density $n_{el}(\mathbf{r})$ the total potential is well screened so that a LL is "pinned" (within $k_BT$) to the electrochemical potential $\mu^*$, which is constant in thermodynamic equilibrium. Neighboring compressible regions, in which adjacentLLs are pinned to $\mu^*$, are separated by an "incompressible" region, in which the potential varies by a cyclotron energy (if we neglect spin-splitting) and no states with energy near $\mu^*$ exist. In such an incompressible region the same number of LLs is fully occupied everywhere, and thus the electron density $n_{el}(\mathbf{r})$ is constant. Since the energy eigenfunctions have a spatial extent of at least the order of the magnetic length $\ell_B = \sqrt{c\hbar/(eB)}$, the picture of alternating compressible and incompressible regions can be correct only if the distance of neighboring compressible regions is everywhere considerably larger than $\ell_B$.

Such ideas of alternating regions with perfect screening (at zero temperature) or no screening have been discussed a long time ago [16] and used to explain experiments revealing an apparent background DOS between LLs [17-20]. Similar arguments have also been used to explain [21] experiments [22-24] on the breakdown of the IQHE under strong currents. The $B$-dependence of position and width of incompressible stripes (ISs) in translation-invariant half plane and stripe geometries have been calculated by Chklovskii *et al.* [14, 15] for a simplified "perfect screening model" at zero temperature. Later self-consistent thermal-equilibrium calculations showed that these ISs, which separate compressible regions, in which neighboring Landau levels are pinned (within $k_BT$) to the spatially constant electrochemical potential, develop already at sufficiently low, but finite temperatures [25, 26]. But, as already discussed previously [27], even if one knows about the position of compressible and incompressible regions in thermodynamic equilibrium, it is not so clear, where an ASDC will flow: in the compressible regions, where states exist near $\mu^*$ and

quasi-elastic scattering is possible, which is important for the stationary transport at $B = 0$, or in incompressible regions, where no empty states near $\mu^*$ exist and such scattering is not possible. In incompressible regions, electric fields and, therefore, Hall currents, exist even in thermal equilibrium, but these cannot lead to dissipation.

In order to investigate the effect of ISs and compressible regions on the spatial distribution of an ASDC, this equilibrium theory was modified by a standard transport theory, assuming that current density and the gradient of the electrochemical potential as driving electric field are connected by a local form of Ohm's law [28, 29]. Moreover, only stationary, current-carrying states were considered, so that the dissipative non-equilibrium states can be described assuming local equilibrium. This results in a strongly non-linear self-consistent theory of screening and magneto-transport, in which the current distribution depends strongly on parameters like magnetic field, temperature, and strength of the ASDC. This theory is able to explain many of the results obtained by mentioned experiments [10-13], as has been explained in detail in several introductory publications [30-32]. We refer to these articles for experimental details and a qualitative comparison of experimental and theoretical results.

The purpose of the present work is to summarize this theory, including some later modifications, which allow discussing Joule heating, as a possible reason for the breakdown of the IQHE, and a lateral modulation of the charge density, as a possible reason for the existence of several parallel ISs with the same filling factor. It will present the basic equations, explain how to solve them numerically, and compare some of its interesting results with the experimental data. This theory gives reasonable results for current distribution and resistances for all temperatures of interest, and the special results observed in the regime of the IQHE are caused by the peculiar screening properties of the 2DES in high magnetic fields at low temperature, i.e., finally by the Coulomb interaction of the electrons, and no assumptions of localization effects are necessary.

The calculations reported in the following discourse are based on the Hartree-type approximations, in which the electron-electron interaction is replaced by the interaction of an electron with the electrostatic field produced by the total 2DES. The exchange and correlation effects and the spin-splitting of Landau levels are neglected. If the exchange effects are considered in a naive approximation, they lead to an unrealistically strong enhancement of the spin-splitting [34] and to the suppression of screening effects [35]. In order to avoid these artifacts and to obtain reasonable results for the exchange-enhancement of spin-splitting and for the effective screening, the self-consistent Hartree-Fock approximation was suggested, in which screening of the interaction potential is also considered in the exchange terms [34, 36]. From such an approximation, one expects similar results for ISs as from a Hartree-type approximation; however, with even and odd integer values of the filling factor, whereas neglect of spin-splitting will always lead to even integer values. The aim of the present review is to recall the explanation of the ISs and their importance for the local distribution of an ASDC. To this end simplifying approximations are made, which reduce the numerical effort enormously but make a quantitative agreement between the calculated and the experimental results impossible. For instance, the assumption of translation invariance can only be a good approximation for the interior of a long sample, far from source and drain contacts. Thus, since we can expect only qualitatively correct results, we also neglect the exchange and correlation effects and spin-splitting; this also simplifies the calculations considerably.

## 2. Thermal Equilibrium

### *2.1 Model*

Our aim is to describe magneto-transport in narrow Hall bars. Due to the lateral confinement, the electron density in such a bar will not be homogeneous but, in general, will decrease from the center of the sample toward its edges. This inhomogeneity of the electron density will lead to the situations, where in different parts of the sample, different numbers of Landau levels will be occupied, and this will affect the current distribution in the sample. In order to describe such situations, we follow previous work [15,26] and model the Hall bar as a two-dimensional system in the plane $z = 0$ with translation-invariance in $y$-direction, metal plates in the half-planes $x < -d$ and $x > d$, and a charge density $\rho(x)\delta(z)$ in the stripe $-d < x < d$, with

$$\rho(x) = e[n_D(x) - n_{el}(x)], \quad (1)$$

where $n_D(x)$ and $n_{el}(x)$ denote the donor and electron densities, respectively, and $-e$ is the charge of an electron. Here the idea is that the metal gates are on the surface of the sample and the donors and electrons occupy different planes in the sample, which are so close to the surface that their distances from the surface are much smaller than the width $2d$ of the stripe between the metal plates, and can be neglected [15, 26]. One can expect that such a model gives a reasonable description of the center region of a long sample, at a sufficiently large distance from the source and drain contacts, which of course destroy the translation invariance.

An advantage of this quasi-two-dimensional model is that the electrostatic potential $V(x,z)$, which, in regions without charges, has to satisfy the Laplace equation, can be explicitly expressed as a function of the boundary conditions at $z = 0$, i.e., the charge density $\rho(x)$ and the constant potential values $V(x,0) = V_L$ and $V(x,0) = V_R$ on the metal gates at $x < d$ and $x > d$, respectively. The mathematical derivation of this result is summarized in Appendix A. Here we need only the resulting potential in the plane $z = 0$, which can be written as the sum of two terms, $V(x,0) = V_G(x,0) + V_C(x,0)$, where

$$V_G(x,0) = \frac{V_R+V_L}{2} - \frac{V_L-V_R}{\pi}\arcsin(\frac{x}{d}) \quad (2)$$

results from the gates and interpolates between the constant gate-potentials, and where

$$V_C(x) = -\frac{2}{\overline{\kappa}}\int_{-d}^{d} dt\ K(x,t)\,\rho(t), \quad (3)$$

with the kernel

$$K(x,t) = ln\ |\ \frac{\sqrt{(d^2-x^2)(d^2-t^2)}+d^2-tx}{(x-t)d}\ |\ , \quad (4)$$

and an effective dielectric constant $\overline{\kappa}$, describes the contribution of the charges in the stripe $z = 0$, $|x| < d$ (compare Appendix A). The normal component of the potential $V_C(x,z)$ on the metal gates leads to induced charges on the gates. The total induced charge on the right gate at $x > d$ is

$$Q_R = -\frac{2}{\pi}\int_{-d}^{d} dt\ \rho(t)\arctan\sqrt{\frac{d+t}{d-t}}\ . \quad (5)$$

The corresponding result $Q_L$ for the left gate is obtained from Eq.(5) by replacing $t$ by $-t$ in the argument of the square root. Thus, the sum of the induced charges, $Q_L + Q_R = -\int_{-d}^{d} dx\rho\,(x)$, compensates the free charges, and their difference vanishes, if the charge density in the Hall bar is symmetric, $\rho(-x) = \rho(x)$ (see Appendix A).

Concerning the self-consistent calculation of electron density and effective potential, we follow most of the previous work and treat this self-consistency problem in the Thomas-Fermi

approximation (TFA), i.e., we assume that relevant macroscopic lengths like the scale on which potential and electron densities vary spatially, are much larger than typical microscopic lengths, like the magnetic length $\ell_B = \sqrt{\hbar/m\omega_c}$, with $\omega_c = eB/(mc)$ the cyclotron frequency, or the extent of Landau eigenfunctions in strong magnetic fields $B$, or like the Fermi wave length or the mean distance between electrons at $B = 0$. In the TFA the electron density is given by

$$n_{el}(x) = \int dE\, D(E)\, f([E + U(x) - \mu^*]/(k_B T)), \quad (6)$$

with $D(E)$ the density of states (DOS) of the 2DES, $f(\epsilon) = 1/[1 + \exp(\epsilon)]$ the Fermi function, $U(x) = -e[V_G(x) + V_C(x)]$ is the effective confinement energy and $\mu^*$ is the constant electro-chemical potential of the thermal equilibrium state. For a Hall bar in the absence of a magnetic field, $B = 0$, we take $D(E) = D_0\theta(E)$, with $D_0 = m/(\pi\hbar^2)$, and for strong, quantizing magnetic fields we take a collision-broadened Landau DOS

$$D(E) = \frac{g_s}{2\pi\ell_B^2}\sum_{n=0}^{\infty} A_n(E), \quad A_n(E) = \frac{1}{\sqrt{\pi}\Gamma}\exp(-\frac{[\varepsilon_n - E]^2}{\Gamma^2}), \quad (7)$$

where $\varepsilon_n = (n + 1/2)\hbar\omega_c$ denotes the Landau energies without spin-splitting and $g_s = 2$ the spin degeneracy. The level broadening is usually taken as $\Gamma = \gamma\hbar\omega_c\sqrt{10\mathrm{T}/B}$ with $\gamma \lesssim 0.1$. This Gaussian model for the spectral function, as the corresponding model for the conductivities [37], which will be given in section 3, is not accurate [34], but gives reasonable results for all temperatures of interest. Another model, the "self-consistent Born approximation" [34], has also been investigated in this context [29] and leads to essentially the same results under the conditions of the IQHE. This is not surprising, since in the IQHE electron scattering is suppressed.

Inserting Eq.(6) into Eq.(3) one obtains the, in general non-linear, integral equation

$$U(x) + \frac{2e^2}{\overline{\kappa}}\int_{-d}^{d} dt\; K(x,t)\,[n_D(t) - n_{el}(t)] = U_G(x) \quad (8)$$

for the effective confinement energy $U(x)$.

### *2.2 Results*

#### 2.2.1 Homogeneous Donor Density

The simplest form of the self-consistency problem occurs for vanishing magnetic field and zero temperature, since Eq.(6) reduces to $n_{el}(x) = D_0\,[\mu^* - U(x)]\theta(\mu^* - U(x))$. If we assume that the electron density is confined to the interval $[x_L, x_R]$, with $-d < x_L < x_R < d$, and anticipate $U(x_L) = U(x_R) = \mu^*$, the self-consistency problem reduces to the linear integral equation [26, 28]

$$U(x) - \frac{1}{\pi a_0}\int_{x_L}^{x_R} dt\, K(x,t)[\mu^* - U(t)] = U_D(x) + U_G(x), \quad (9)$$

where $a_0 = \overline{\kappa}\hbar^2/(2me^2)$ is a screening length. $U_G(x) = -eV_G(x,0)$ describes the effect of the metal gates, see Eq.(2), and $U_D(x) = -E_0\sqrt{1 - x^2/d^2}$ with $E_0 = 2\pi e^2 n_0 d/\overline{\kappa}$ describes the bare confinement energy provided by the donors, which, for constant donor density $n_D(x) = n_0$, is given by Eq.(31).

The efficiency of screening depends strongly on the screening parameter

$$\alpha = \pi a_0/d. \quad (10)$$

The smaller the value of $\alpha$, the more effective becomes the screening [26].

In the following sections, we use the parameters adjusted to GaAs/AlGaAs samples, i.e., $D_0 = 2.79 \cdot 10^{10}/(\mathrm{meV\ cm^2})$ for the $(B = 0)$-DOS and $2a_0 = 9.79$ nm for the effective Bohr radius [29]. Then, for constant donor density $n_D(x) = n_0 = 4 \cdot 10^{11}\ \mathrm{cm^{-2}}$ and $d = 1.5\,\mu$m, which leads to $E_0 = 2\pi e^2 n_0 d/\overline{\kappa} = 4.377$eV, we obtain $\alpha = 0.01$ and the results of Figure 1. Here we assumed

vanishing gate-potential, $V_L = V_R = 0$, and anticipated that the constant donor density will lead, in thermal equilibrium, to a symmetric electron density, $n_{el}(-x) = n_{el}(x)$. Apparently the bare confinement potential $U_D(x) = -E_0\sqrt{1 - x^2/d^2}$, created by the donors and indicated by green lines in Figure 1, is heavily screened by the 2DES, so that the screened effective confinement potential appears nearly flat in the region occupied by electrons.

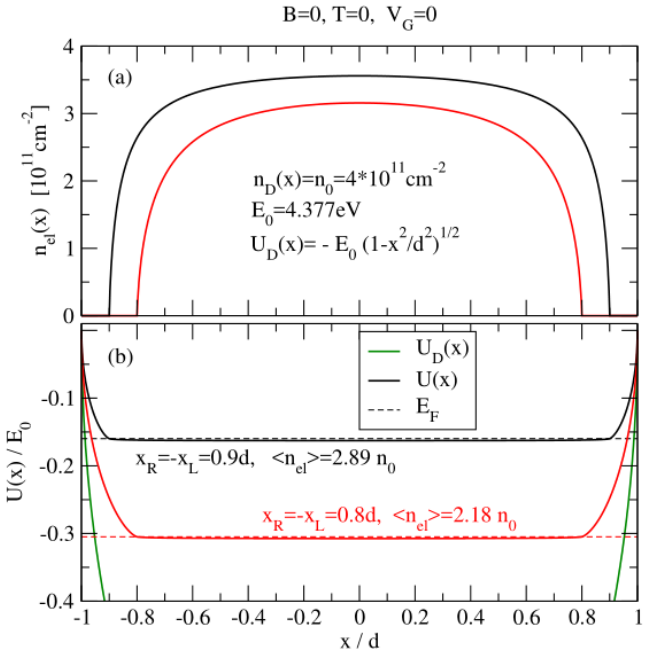


**Figure 1** Self-consistent solutions of Eq.(9) for the constant donor density $n_D(x) = n_0 = 4 \cdot 10^{11}\,\mathrm{cm}^{-2}$ and two symmetric choices of the electron distribution. (a) Electron densities $n_{el}(x)$, (b) effective confinement potentials $U(x)$ (solid lines) and chemical potentials $\mu^* = E_F$ (dashed lines); $d = 1.5\,\mu$m, $\alpha = 0.01$.

At finite temperature Eqs.(6) and (8) lead to a non-linear integral equation, to solve by the Newton-Raphson iteration method. One starts with a suitable approximation $U_0(x)$ of the desired solution $U(x)$, writes $U(x) = U_0(x) + \Delta(x)$ in the integral equation, assumes $\Delta(x)$ to be small, and linearizes it with respect to $\Delta(x)$. The solution of the linear integral equation for $\Delta(x)$ is added to $U_0(x)$, and the sum is taken as new starting approximation. In each iteration step the average electron density

$$< n_{el} >= \frac{1}{2d}\int_{-d}^{d} dx\; n_{el}(x) \quad (11)$$

is kept constant. The iteration usually converges, if the starting value $U_0(x)$ is close enough to the solution. The results of Figure 2 are obtained in this manner, starting with the result for $B = 0$, $T = 0$, and $x_R = -x_L = 0.9d$, shown in Figure 1 and in Figure 2 as black lines. Starting with this, the result for $B = 0$ and $T = 50\mathrm{K}$ (red lines) was calculated. This took many iterations but converged with high accuracy. Starting from this result, the calculation for $B = 7\mathrm{T}$ and $T = 50\mathrm{K}$ (broken blue lines) took only a few iterations. To get the results for $B = 7\mathrm{T}$ and lower temperatures, $T$ was lowered in small steps, and in each step, only a few iterations were needed. Since the problem is symmetric,$n_{el}(-x) = n_{el}(x)$ and $U(-x) = U(x)$, Figure 2 shows only results for $-d < x < 0$. Parts (a) and (b) in Figure 2 refer to the electron density and panels (c) and (d) to the self-consistent confinement potential. Apparently the overall changes in the electron density profile with

changing temperature and magnetic field are relatively small, but the inset in Figure 2(a) shows, that the sharp onset of $n_{el}(x)$, seen for $T = 0$ at $x = -0.9d$, is broadened at finite temperatures. Most important for the following is the appearance of incompressible stripes (ISs) near $x = \pm 0.53d$ for$B = 7\mathrm{T}$ and $T \lesssim 4\mathrm{K}$. As part (b) and (d) show (for $T = 1.5\mathrm{K}$), an IS occurs where the chemical potential is located well between the two lowest Landau energy bands $\varepsilon_0(x)$ and $\varepsilon_1(x)$, where $\varepsilon_n(x) = U(x) + \hbar\omega_c(n + 1/2)$. Since we neglect spin-splitting, these ISs have local filling factor $\nu(x) = 2$. Figure 2(c) shows the enlarged part of the interesting region of $U(x)$. For $|x| > 0.9d$ these curves are nearly equal and increase monotonously towards $U(\pm d) = 0$.

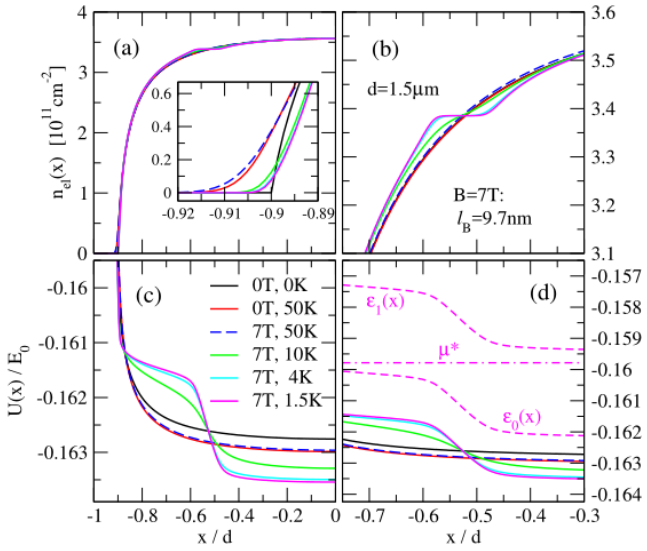


**Figure 2** Electron density, (a) and (b), and screened confinement potential, (c) and (d), for $B = 0$ and temperatures $T = 0$ and $T = 50\mathrm{K}$, and for $B = 7\mathrm{T}$ and several temperatures, as indicated. Parameters $x_R = -x_L = 0.9d$, $d = 1.5\,\mu\mathrm{m}$, $n_0 = 4 \cdot 10^{11}\mathrm{cm}^{-2}$, $< n_{el} >= 2.89n_0$, $\alpha = 0.01$. For $B = 7\mathrm{T}$ the DOS is taken from Eq.(7) with $g_s = 2$ and $\gamma = 0.1$.

Figure 2 demonstrates nicely that near the sample edges, where the electron density decreases rapidly, the effective confinement potential shows a characteristic spatial variation, even for vanishing temperature and magnetic field. This potential variation, which is small compared with its variation between the center of the stripe (at $x = 0$) and the metal gates (at $x = \pm d$), was neglected in the "perfect screening approximation" [14, 15], to enable an analytical solution of the problem. Near the sample edges, these analytical solutions deviate considerably from the results of the self-consistent treatment, but far from these edges, nearly the same results for the position and width of the ISs are obtained. This has been discussed in detail in an earlier study [25].

The width of the ISs and the pinning of the Landau bands to the electrochemical potential $\mu^*$, shown in the right panels of Figure 2, become more impressive, if a smaller collision broadening is considered [38]. This is shown in Figure 3(a), which indicates the lowest Landau bands for $B = 7\mathrm{T}$, $T = 1.5\mathrm{K}$ and two values of the collision broadening. For the smaller value, $\gamma = 0.01$ (red lines), the energy bands $\varepsilon_0(x)$ and $\varepsilon_1(x)$ are closely pinned to the electrochemical potential and the ISs are wider than for the larger collision broadening $\gamma = 0.1$ (green lines). In general, the width of the ISs

decreases with increasing temperature and increasing collision broadening, and for $k_BT/\hbar\omega_c \gtrsim 0.04$ and $\Gamma/\hbar\omega_c \gtrsim 0.1$ no ISs exist [27].

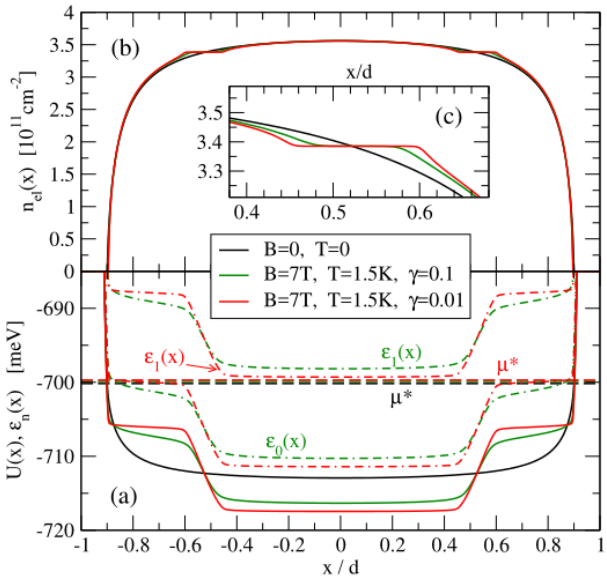


**Figure 3** Self-consistent potential (a) and electron density (b) in thermal equilibrium. Black lines are for $B = 0$, $T = 0$; other lines for $B = 7\text{T}$, $T = 1.5\text{K}$ and two values of the Landau level broadening, $\gamma = 0.1$ (green) and $\gamma = 0.01$ (red); other parameters as in Figure 2. Broken lines: $\mu^*$; dash-dotted lines: Landau energy bands. The inset (c) shows $n_{el}(x)$ near $x = 0.52d$.

In view of the ISs, a modification of the TFA should be mentioned, that was used in most of the numerical calculations. Replacing the Hartree approximation by the TFA, one neglects the spatial extent of the Landau eigenfunctions, which for the low-energy eigenfunctions is of the order of the magnetic length $\ell_B$. As a consequence, the TFA may predict very narrow ISs, which are not reliable. Careful investigations of several modifications of the Hartree approximation [29, 33] showed, that the TFA gives reasonable results, if in each iteration step the quantities, which in principle are determined by eigenfunctions, are averaged spatially over a length of the order of $\ell_B$, i.e., if one replaces $n_{el}(x)$ by

$$n_{el}(x) = \frac{1}{2\lambda}\int_{-\lambda}^{\lambda} dt\; n_{el}(x+t), \quad (12)$$

for instance with $\lambda = \ell_B$. This modification was used in the calculation of Figure 2, but not in Figure 3, and will be used in the following. For $B = 7\text{T}$, i.e., $\ell_B = 9.7$ nm, one obtains ISs with $\nu(x) = 2$ of a width $\Delta_{(7;2)} \gtrsim 100$ nm. When $B$ becomes larger, the ISs become wider and move towards the center $x = 0$. For $B > 7.4\text{T}$ the filling factor in the center becomes less than 2, $\nu(0) < 2$, and no ISs exist. As $B$ decreases, the ISs become narrower and move towards the sample edges.

A survey over the $B$-dependence of position and width of the ISs is given in Figure 4. Panel (a) of the figure shows parts of the $n_{el}(x)$-profiles for four $B$-values. For $B = 6\text{T}$ and $B = 7\text{T}$, ISs with filling factor $\nu(x) = 2$ occur near $x = 0.76d$ and $x = 0.53d$, respectively. For $B = 3\text{T}$ and $B = 3.5\text{T}$, one finds somewhat smaller ISs with $\nu(x) = 4$ centered at the same positions. For these $B$-values one might expect ISs with $\nu(x) = 2$ near $x = 0.88d$ and $x = 0.87d$, respectively, but these ISs are

not well developed. Since these $n_{el}(x)$ profiles fall very close together, Figure 4(b) shows the filling factor profiles $\nu(x)$ for a larger number of $B$-values.

Because the model has the symmetry $n_{el}(-x) = n_{el}(x)$, Figure 4(b) shows only data for $-d < x < 0$. For $B = 6\text{T}$, where $\ell_B = 10.5$ nm, one finds for the ISs near $x = \pm 0.76d$ a width $\Delta_{(6;2)} \approx 61$ nm. With further decreasing $B$, the width of the ISs rapidly decreases, until no ISs with filling factor $\nu(x) = 2$ exist anymore. For $B = 3.5\text{T}$, where $\ell_B = 13.7$ nm, no ISs with $\nu(x) = 2$ can be clearly identified, but near $x = \pm 0.53d$ narrow ISs with filling factor $\nu(x) = 4$ and width $\Delta_{(3.5;4)} \approx 81$ nm exist, which are embedded in the $(\nu = 2)$-ISs for $B = 7\text{T}$ of width $\Delta_{(7;2)} \approx 153$ nm.

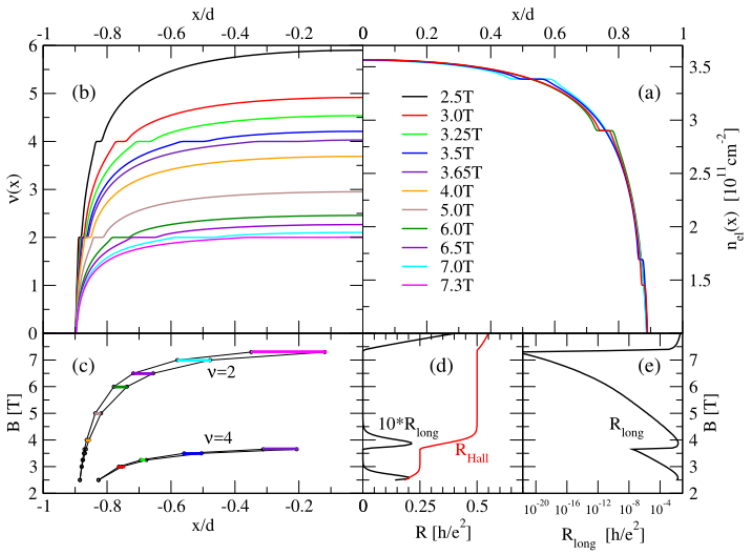


**Figure 4** Electron density $n_{el}(x)$ for $B = 3\text{T}$, 3.5 T, 6 T, and 7 T (a) and filling factor $\nu(x)$ for the indicated $B$-values (b); part (c) shows for these $B$-values the position of the incompressible strips, part (d) the calculated longitudinal and Hall resistance in linear, and (e) the longitudinal resistance in logarithmic scale. $T = 1.5\text{K}$, $\gamma = 0.05$ and other parameters as in Figure 2.

In Figure 4(c) the vertical axis presents the magnetic field and, for the $B$-fields considered in Figure 4(b), the positions of the corresponding ISs are indicated. This plot is similar to the experimental plots describing the $B$-dependence of the local current distribution in a narrow Hall bar under the conditions of the IQHE [12, 30-32].

In order to emphasize the relation between ISs and the IQHE, Figures 4(d) and 4(e) show the $B$-dependence of the resistances in linear response approximation, calculated with the formalism, which will be introduced in section 3. Figure 4(d) shows longitudinal and Hall resistance on a linear scale, 4(e) shows the longitudinal resistance on a logarithmic scale. In Figure 4(d), we see two quantum Hall plateaus, where the Hall resistance has the quantized values $R_{\text{Hall}} = h/(ne^2)$ with $n = 2$ and $n = 4$, and where $R_{\text{long}}$ vanishes. Apparently the quantization is more pronounced in the plateau with $n = 2$ than in the plateau with $n = 4$. If we consider the quantization to be well pronounced when $R_{\text{long}} < 10^{-4} h/e^2$, the quantum Hall plateau with $n = 4$ covers the interval $3.1\text{T} \lesssim B \lesssim 3.6\text{T}$, and the plateau with $n = 2$ the interval $4.6\text{T} \lesssim B \lesssim 7.35\text{T}$. A comparison of Figures 4(b) and 4(c) shows that, in the $B$-regime considered in Figure 4, well developed ISs exist only for $B$-values in these quantum Hall plateaus.

### 2.2.2 Modulated Donor Density

In the analytical model of zero-temperature screening [14, 15] one finds, that the width $\Delta(x_0)$ of an IS centered at $x = x_0$ is inversely proportional to the slope of the zero-$B$ electron density at this center, $\Delta(x_0) \propto |\frac{dn_{el}}{dx}(x_0)|^{-1}$. This anticipates qualitatively the numerical results just discussed. Early scanning force microscopy experiments [11, 12] on narrow Hall bars showed that, under the conditions of the IQHE, the ASDC flows through stripes, which change position and width as a function of the applied magnetic field in just this manner. Thus it seemed that the current flows through these ISs, as will be discussed in the following chapter. The later experiments [38, 39] showed that, for magnetic fields in the high-$B$ part of a quantum-Hall-plateau (QHP), the ASDC can flow through a wider region than through ISs near the center of the sample. In order to describe such situations, a model with a modulated donor density has been considered.

$$n_D(x; w) = n_0[1 + w\cos(k_D\pi x/d)] \quad (13)$$

Some results for $n_0 = 4 \cdot 10^{11}\text{cm}^{-2}$, $w = 0.1$ and $k_D = 5$ have been published some time ago [39], and some for $n_0 = 4 \cdot 10^{11}\ \text{cm}^{-2}$, $w = -0.1$ and $k_D = 1$ more recently [40]. For these models the electron densities at $B = 0$ and $T = 0$, calculated from the linear integral equation (9) with

$$U_D(x) = -\frac{E_0}{\pi d}\int_{-d}^{d} dt\ K(x,t)[1 + w\cos(k_D\pi t/d)], \quad (14)$$

are plotted in Figure 5. Because the donor densities have the symmetry $n_D(-x) = n_D(x)$, the electron densities have the same symmetry. Therefore we show for $k_D = 5$ (the right panels of Figure 5), only one half of the results, the interval $-d < x < 0$ for $w = 0.1$ and $0 < x < d$ for $w = -0.1$. For comparison, the corresponding results for constant donor density, $w = 0$, are indicated by black lines.

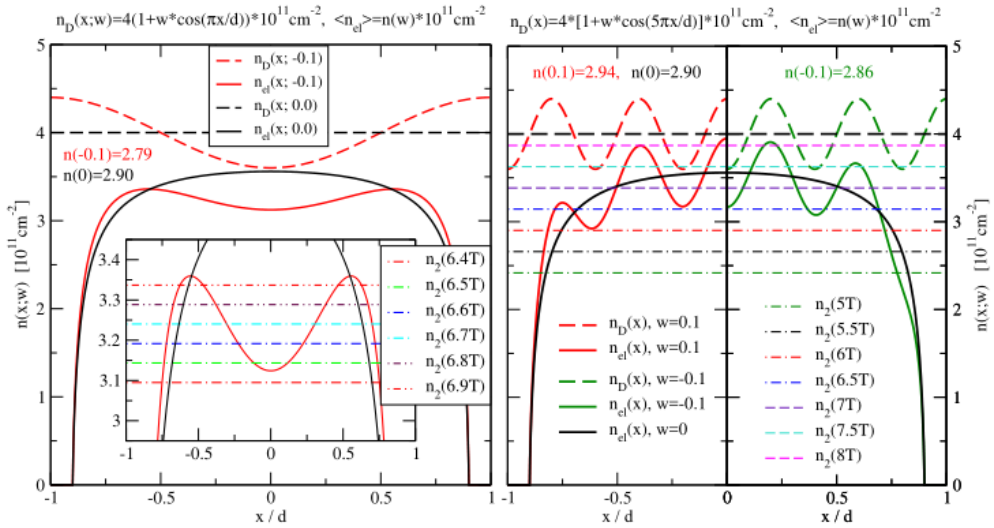


**Figure 5** Symmetric donor densities according to Eq.(13), with $n_0 = 4 \cdot 10^{11}\ \text{cm}^{-2}$, and with $k_D = 1$ and $w = -0.1$ (left), and with $k_D = 5$ and $w = 0.1$ (medium) and $w = -0.1$ (right panel), respectively, and, for $B = 0$ and $T = 0$, the corresponding electron densities, satisfying $n_{el}(x) = 0$ for $|x| > 0.9d$ and $n_{el}(x) > 0$ for $|x| < 0.9d$. Black lines indicate the corresponding results for $w = 0$. The horizontal dash-dotted line $n_2(B)$ indicates the density, leading at magnetic field $B$ to filling factor $\nu = 2$.

The dash-dotted horizontal line $n_2(B)$ in Figure 5 indicates the electron density, at which in the magnetic field of strength $B$, the filling factor of Landau levels becomes $\nu = 2$. Where these lines cross the $n_{el}(x)$ profile, an IS may develop at sufficiently low temperatures. Whereas for the constant donor density ($w = 0$) for a given $B$-field at most two ISs with filling factor $\nu(x) = 2$ can exist, for the donor modulation with $k_D = 1$ up to four ISs are possible. For the modulations with $k_D = 5$ in certain $B$-intervals up to eight ISs are possible, and for $w = 0.1$ in a narrow $B$-interval around $B = 6.6$T even ten ISs with $\nu(x) = 2$ seem to be possible. If for a given $B$-value $n_2(B)$ has several crossings with the profile $n_{el}(x)$ and the slope $\frac{dn_{el}}{dx}(x)$ is different at different crossing points, the ISs at these crossing points will have different widths. As an example, Figure 6 shows, for several temperatures, the self-consistently calculated electron density and effective confinement potential for the modulation with $k_D = 5$ and $w = 0.1$, for $B = 0$ and $B = 7$ T. The other parameters are chosen as shown in Figure 2. As in this figure, the overall appearance of the density profile does not change very much as function of $B$ and $T$, but the onset of finite electron density $n_{el}(x)$ near $x = \pm 0.9d$ is smooth at finite temperature, as shown by the inset of (a), and for $B = 7$ T and temperatures $T \lesssim 4$K six ISs develop near $x/d = \pm 0.13$, $\pm 0.27$ and $\pm 0.51$, as shown in (b). Due to the screening effects, the self-consistent confinement potential and, as a consequence, the Landau energy bands $\varepsilon_n(x) = U(x) + \hbar\omega_c(n + 1/2)$, show at $T \lesssim 4$K considerably stronger oscillations than those at high temperatures.

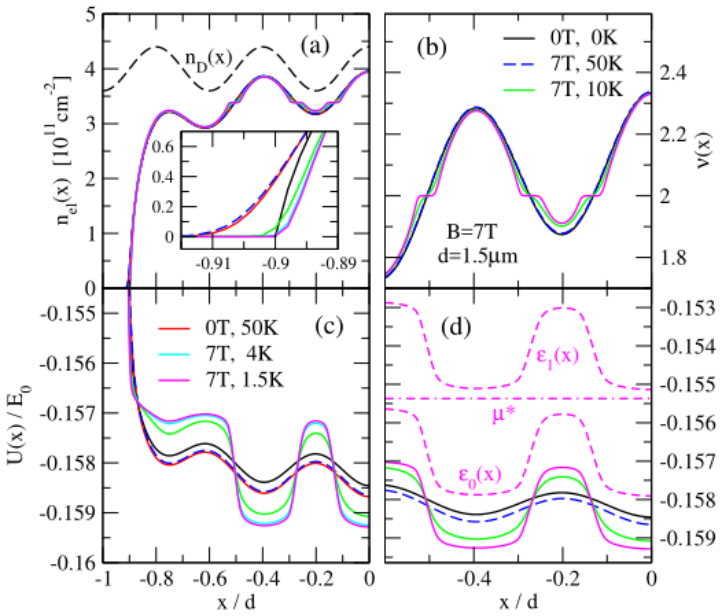


**Figure 6** Electron density, (a) and (b), and effective confinement potential, (c) and (d), for $B = 0$ and $B = 7$ T and several temperatures, calculated for the donor density modulation given by Eq.(13) with $n_0 = 4 \cdot 10^{11}$ cm$^{-2}$, $k_D = 5$ and $w = 0.1$, and other parameters as in Figure 2.

### 2.2.3 Equilibrium Currents

In the Landau gauge, the planar eigenfunctions in a constant, perpendicular magnetic and an in-plane constant electric field carry a constant in-plane current perpendicular to both fields. For a 2DES, laterally confined in $x$-direction and translation-invariant in $y$-direction, this leads to edge-

currents, which can be described by the eigenfunctions, if the confinement potentials vary sufficiently smoothly. In the situations considered so far, the opposite edge-currents at opposite edges cancel each other. It is, however, possible to describe with the formalism of section 2.1, a dissipation-free equilibrium current, if one adds to the argument of the Fermi function in Eq.(6) a suitable term proportional to the required net current. The consequences of such a theory have been discussed by several authors [41, 26], but they cannot explain the measured distribution of an ASDC in narrow Hall bars, and also not the transition of a 2DES in such a Hall bar from a normal, dissipative state at higher temperatures to a state dominated by the IQHE at low temperatures.

## 3. Stationary Magneto-Transport Theory

### *3.1 Local Version of Ohm's Law*

In order to understand the experimental results on the spatial distribution of the ASDC in a narrow Hall sample, a theory is needed that describes the normal dissipative situation of the sample at higher temperatures (up to room temperature) as well as the low-temperature limit, where the sample shows the IQHE. Such a theory has been developed [27-29, 38] under the usual assumption, that a *stationary non-equilibrium* state can be described as a state with a *local thermal equilibrium*, which is justified if the spatial variations of electron and current densities are smooth enough. According to the rules of non-equilibrium thermodynamics one expects that in the resulting stationary state the entropy production is minimal.

A stationary current, imposed on a laterally confined 2DES, will lead to position-dependent current densities and electric fields. Following previous work [28], we assume that the relevant electric field, driving the density $\mathbf{j}(\mathbf{r})$ of the imposed current, is the gradient of the electrochemical potential, $\boldsymbol{\nabla}\mu^*(\mathbf{r})$, which vanishes in thermal equilibrium. In the presence of an ASDC, on the other hand, the $\mu^*$ in Eq.(6) becomes position-dependent. Local equilibrium means that all thermodynamic quantities satisfy locally the same interrelations as they do in a homogeneous system. So, current density $\mathbf{j}(\mathbf{r}) = (j_x(x,y), j_y(x,y))$ and electric field should satisfy a local version of Ohm's law,

$$\hat{\rho}(\mathbf{r})\mathbf{j}(\mathbf{r}) = \mathbf{E}(\mathbf{r}) \equiv \boldsymbol{\nabla}\mu^*(\mathbf{r})/e, \quad (15)$$

where the local resistivity tensor $\hat{\rho}(\mathbf{r}) = [\hat{\sigma}(\mathbf{r})]^{-1}$, with components $\rho_{xx}(x) = \rho_{yy}(x) = \rho_l(x)$ and $\rho_{xy}(x) = -\rho_{yx}(x) = \rho_H(x)$, is the inverse of the local conductivity tensor, which should be calculated in an approximation that is consistent with that for the electron density.

With translation invariance in $y$-direction, $\hat{\rho}$, $\mathbf{j}$ and $\mathbf{E}$ are independent of $y$ and the Maxwell equations $\boldsymbol{\nabla}\cdot\mathbf{j}(\mathbf{r}) = 0$ and $\boldsymbol{\nabla}\times\mathbf{E}(\mathbf{r}) = \mathbf{0}$ require, that the current density $j_x$ across and the electric field $E_y$ along the bar are independent of $x$,

$$j_x(x) \equiv j_x^0 = 0, \quad E_y(x) \equiv E_y^0. \quad (16)$$

Then the electrochemical potential assumes the form $\mu^*(x,y) = \mu^*(x) + eE_y^0 y$ and, in order to guarantee the translation invariance in $y$-direction, we must add in Eq.(6) to the confinement energy $U(x)$ a term $eE_y^0 y$, which describes the effect of the source-drain voltage along the Hall bar. Since in the argument of the Fermi function, only the difference $U(x,y) - \mu^*(x,y) = U(x) - \mu^*(x)$ occurs, the electron and current density as well as the transport coefficients to be calculated below, are independent of $y$ [27].

We consider only Hall bars, in which the electron density vanishes near the edges, so that no current can flow through the edges, $j_x^0 = 0$. Then Ohm's law simplifies to

$$j_y(x) = E_y^0/\rho_l(x), \quad E_x(x) = \rho_H(x)\, j_y(x), \text{ (17)}$$

resulting in $\mu^*(x,y) = \mu^*(x) + eE_y^0 y$ with

$$\mu^*(x) = \mu_0^* + eE_y^0 \int_0^x dx'\ \rho_H(x')/\rho_l(x'). \text{ (18)}$$

Here $\mu_0^*$ occurs as a constant determining the average electron density, and $E_y^0$ is determined by the total ASDC, $I = \int_{-d}^{d} dx\ j_y(x)$, as

$$E_y^0 = I/\int_{-d}^{d} dx\,[1/\rho_l(x)]. \text{ (19)}$$

If in the limit $T \to 0$, an IS develops in the Hall bar, where $\rho_l(x) \to 0$, the last integral becomes extremely large and the electric field and thus the resistance along the Hall bar becomes extremely small, and the sample shows the IQHE. But it is clear that this formalism does not work at $T = 0$, since then the relevant integrals diverge.

Equation (19) yields the longitudinal resistance, calculated for a square geometry with $\Delta y = \Delta x = 2d$ as

$$R_{\text{long}} = \frac{2dE_y^0}{I} = 2d/\int_{-d}^{d} dx \frac{1}{\rho_l(x)} \text{ (20)}$$

The Hall resistance follows from Eq.(18) as

$$R_{\text{Hall}} = [\mu^*(d) - \mu^*(-d)]/(eI) = \int_{-d}^{d} dx \frac{\rho_H(x')}{\rho_l(x')} / \int_{-d}^{d} \frac{dx}{\rho_l(x)} \text{ (21)}$$

### *3.2 Conductivity Model*

#### 3.2.1 Homogeneous 2DES

The scattering of electrons by randomly distributed impurities leads to both, a collision broadening of the electronic DOS and resistance against electronic current, and, as a consequence, to dissipation. Since electron and current densities are related by the equation of continuity, the calculation of DOS and conductivities should obey certain consistency requirements, the so-called Ward identities [42]. These requirements are, e.g., satisfied by the self-consistent Born approximation, which, together with other approaches, is discussed in the review article by Ando, Fowler and Stern [34] and has also been summarized in the present context [29]. Here we use another approximation scheme, which relies on a cumulant expansion [37], is mathematically easier to handle, and was used in most of our previous work [28, 38, 43].

In order to calculate the resistivity components $\rho_l = \sigma_l/(\sigma_l^2 + \sigma_H^2)$ and $\rho_H = \sigma_H/(\sigma_l^2 + \sigma_H^2)$, we need the conductivity components $\sigma_l = \sigma_{xx} = \sigma_{yy}$ and $\sigma_H = \sigma_{yx} = -\sigma_{xy}$. For a homogeneous system at temperature $T$ in a sufficiently strong magnetic field $B$, we approximate these, using the filling factor $\nu = 2\pi\ell_B^2\, n_{el}$, by

$$\sigma_H = (e^2/h)\nu, \quad \nu = 2\int_{-\infty}^{\infty} dE \sum_{n=0}^{\infty} A_n(E) f([E + U - \mu^*]/k_B T),$$
$$\sigma_l = \frac{e^2}{h}\int_{-\infty}^{\infty} dE[-f'_E] \sum_{n=0}^{\infty}(2n+1)[\sqrt{\pi}\Gamma A_n(E)]^2, \text{ (22)}$$

where $A_n(E)$ is the spectral function from Eq.(7), $f(\varepsilon) = 1/[1 + \exp(\varepsilon)]$ the Fermi function, $f'_E = df([E + U - \mu^*]/k_B T)/dE$ and $\mu^*$ the constant chemical potential. For a homogeneous system, $U$ is an unimportant constant fixing the energy zero.

Figure 7 shows, for constant magnetic field $B$ and for the indicated constant values of temperature ($t = k_B T/\Omega$) and collision broadening ($\gamma_0 = \Gamma/\Omega$), the filling factor $\nu(\mu^*)$ and the

longitudinal conductivity $\sigma_l(\mu^*)$ as functions of the chemical potential (upper panel, with $U = 0$ and $\Omega = \hbar\omega_c$) and $\sigma_l$ as function of $\nu$ (lower panel), see also [27, 28]

It is important in the present context to mention that this approximation describes the Shubnikov – de Haas effect. If the collision broadening of $A_n(E)$ is sufficiently small, at integer (here even) values of the filling factor $\nu$, the chemical potential lays between two Landau levels and, at sufficiently low temperatures, $\sigma_l$ becomes extremely small. This effect, which becomes more pronounced with decreasing temperature and collision broadening and disappears at high temperatures and large collision broadening of the Landau levels, is important for our understanding of the IQHE in narrow samples.

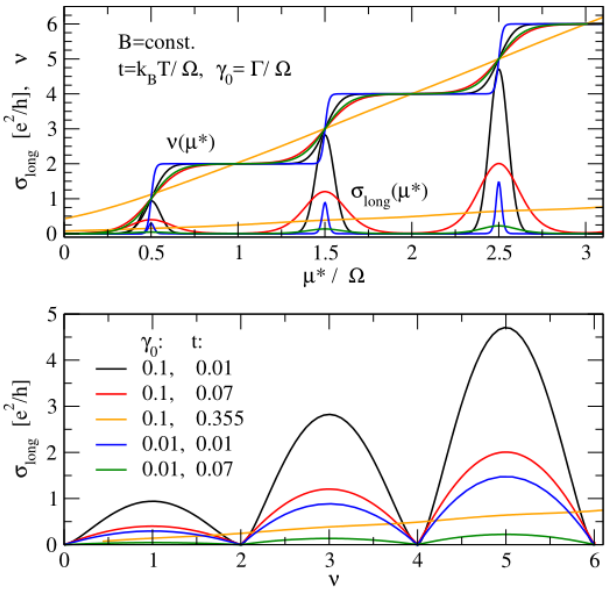


**Figure 7** Filling factor $\nu$ and longitudinal conductivity $\sigma_l$ as function of the chemical potential $\mu^*$ (upper panel) for a homogeneous 2DES in a constant $B$-field at constant temperature $T$ for the indicated values $t = k_BT/\Omega$ and collision broadening $\gamma_0 = \Gamma/\Omega$, after Eq.(22) with $\Omega = \hbar\omega_c$ and $U = 0$. The lower panel shows the corresponding conductivity values as function of the filling factor.

### 3.2.2 Laterally Confined, Translation-Invariant 2DES

Due to the lateral confinement in $x$-direction, the electron density of our model system, which is assumed to be translation-invariant in $y$-direction, decays towards the edges at $x = \pm d$. If this decay is sufficiently smooth, i.e., if $d$ is sufficiently large, we can apply the Thomas-Fermi approximation and use Eqs.(22) replacing $U$ by $U(x)$, the energy due to the effective confinement potential. This yields then position dependent values, $\sigma_H(x)$ and $\sigma_l(x)$, for the conductivities. In order to avoid the artifacts of the Thomas-Fermi approximation, such as ISs of extremely small width, we replace the local conductivities $\sigma_{\mu\nu}(x)$ by the smoothened form

$$\overline{\sigma}_{\mu\nu}(x) = \frac{1}{2\lambda}\int_{-\lambda}^{\lambda} d\xi\ \sigma_{\mu\nu}(x+\xi), \quad (23)$$

in analogy to Eq.(12). With these smoothed values, we calculate the resistivities $\rho_l(x) = \overline{\sigma}_l(x)/[\overline{\sigma}_l(x)^2 + \overline{\sigma}_H(x)^2]$ and $\rho_H(x) = \overline{\sigma}_H(x)/[\overline{\sigma}_l(x)^2 + \overline{\sigma}_H(x)^2]$ needed in Sec.3.1.

*Thermal equilibrium.* If we consider thermal equilibrium in the absence of dissipative currents, temperature, and chemical potential are spatially constant, and we can use Eqs.(22) with $U = U(x)$ and constant $T$ and $\mu^*$, as we did in section 2. The results can also be used to calculate resistances for extremely small ASDCs, in the linear response regime, as we will do in section 4.1 below.

*Weak currents.* According to section 3.1, a finite ASDC leads to a position-dependent electrochemical potential $\mu^*(x)$. If the current is weak enough, the effects of dissipation and Joule heating may be small and negligible. Then one can use Eqs.(22) with spatially constant temperature $T$ and position-dependent values of $U(x)$ and $\mu^*(x)$. This approximation was used to explain the current-induced asymmetries of electron and current densities [27-29]. It is, however, not able to explain the breakdown of the IQHE caused by strong currents.

*Dissipative currents.* Assuming local equilibrium with a stationary current density $j_y(x)$, we should take into account the local Joule heating $W(x) = E_y^0\, j_y(x)$, which will lead to a local enhancement of the electron temperature. In a stationary state of the 2DES, the produced heat must be transferred to the surrounding lattice. Here we neglect the possibility of heat flow within the 2DES and take only the direct local heat transfer $P_L(x)$ to the lattice into account, which will depend on the difference between the local electron temperature $T_{el}(x)$ and the homogeneous lattice temperature $T_L$. Assuming this difference sufficiently small, we take from the literature [44] the linearized form $P_L(x) = C_p^0\, D_T(x)[T_{el}(x) - T_L]$, where $C_p^0 = (k_B/\hbar)\, 10^{-3}(\text{meV})^2$ describes the effect of electron-phonon scattering and $D_T(x) = \partial n_{el}(x)/\partial \mu^*(x)$ denotes the thermal density of states at position $x$. The balance of Joule heating and heat transfer to the lattice then yields for the local electron temperature [43]

$$T_{el}(x) = T_L + \Delta T(x), \quad \Delta T(x) = (2p/C_p^0)\, E_y^0\, j_y(x)/D_T(x), \tag{24}$$

where a parameter $p$ for the coupling strength is introduced ($p = 0.5$ is taken in [44] and $p = 0$ neglects Joule heating).

### *3.3 Calculation Procedure*

A typical problem, we want to calculate, is the current distribution in a Hall bar with a given value of the average electron density at given values of magnetic field $B$, lattice temperature $T_L$ and applied current $I$. In all considered situations we assume the simple model discussed in section 2.1 with translation invariance in $y$-direction and a symmetric donor density $n_D(-x) = n_D(x)$. We start the calculation assuming $B = 0$, $T_L = 0$ and $I = 0$, i.e., the problem discussed in Sec.2.2 and choose the interval $x_L < x < x_R$ with $x_L = -x_R$ so that the average electron density $< n_{el} >$ has the desired value. Then, still with $I = 0$, we increase $T_L$ so much, that we can introduce the desired value of $B$ with the Newton-Raphson iteration described in Sec.2.2. Now we have two possibilities to proceed. First, we can introduce the desired current stepwise at the high $T_L$ and then lower, with the desired values of $B$ and $I$.

Somewhat simpler is the second way [27]. We decrease the temperature with $I = 0$ and the desired value of $B$, as described in Sec.2.2, until we reach the desired value of $T_L$. Then, with $I = 0$, there is no Joule heating, and electron temperature $T_{el}(x) \equiv T_L$ and electrochemical potential $\mu^*$ are spatially constant. With these results, we can calculate the resitivity components $\rho_H(x)$ and $\rho_l(x)$ as described in Sec.3.2. If the ASDC $I$ is very small, $I \to 0$, one is in the linear response limit and the resistances are given by Eqs.(20) and (21).

For finite $I$, one uses the resistivity components calculated according to Sec.3.2 and calculates $\mu^*(x) - \mu_0^*$ from Eqs.(18) and (19) as well as the electron temperature $T_{el}(x)$ from Eq.(24) using Eq.(19) and $D_T(x) = \partial n_{el}(x)/\partial \mu^*(x)$ with $n_{el}(x)$ calculated from Eq.(6). Then one replaces, for the following, Eq.(6) by

$$n_{el}(x) = \int dE\, D(E)\, f([E + U(x) - \mu^*(x)]/[k_B T_{el}(x)]). \quad (25)$$

With this, one has to solve the non-linear integral equation for $U(x)$, Eq.(8) with Eq.(6), keeping the average electron density $< n_{el} >$ and the induced charge $Q_R$, Eq.(35), fixed. This determines the constant $\mu_0^*$. For the solution of the integral equation with fixed $\mu^*(x) - \mu_0^*$, one uses again the Newton-Raphson iteration. With the solution $U(x)$ and $\mu^*(x)$, one calculates again the local resistivity components and a new value of $\mu^*(x) - \mu_0^*$. If this agrees, within the required accuracy, with the previous value, the calculation for this value of $I$ is ready. If not, one inserts the new value into Eq.(25) and solves the integral equation again and calculates a new $\mu^*(x) - \mu_0^*$, until the required accuracy is reached. For larger values of $I$, it may be necessary to approach this value stepwise, with sufficiently small steps, and to achieve convergence in each step.

If one uses the first mentioned possibility and introduces $I$ at the desired $B$ and high $T_L$, one has to obey Eq.(25) to obtain convergence in each step, while approaching the desired value of $I$ at high $T_L$ and while lowering $T_L$ at the desired value of $I$.

## 4. Results

### *4.1 Weak Applied Currents*

If the ASDC is sufficiently small, one can neglect its feedback on electron density, transport coefficients and local electron temperature, and calculate these quantities for $I = 0$. As already mentioned, the occurrence of the IQHE is closely related to the occurrence of ISs. The existence and width of the ISs depend not only on magnetic field and temperature, but also on the collision broadening of the Landau DOS. The width of ISs and the $B$-dependence of Hall and longitudinal resistance, especially the width of the ($\nu = 2$)-QHP, have been investigated [29] on the basis of the self-consistent Born approximation and a special impurity model. The results are compatible with those [27, 38, 43] for the Gaussian model, Eqs.(7), (22) and (23). The resistance results for a modulated system, Eq.(13) with $k_D = 1$ and $w = -0.1$, have also been published [40] and are consistent with those shown in Figure 8, which shows the linear response resistance for the models with $k_D = 5$ described in Figure 5. Figure 8 shows Hall and longitudinal resistance as a function of the magnetic field for two temperatures and for two donor-density modulations with the indicated parameters $w = 0.1$ (red lines) and $w = -0.1$ (green lines). Black lines refer to the unmodulated case $w = 0$. For $T = 1.5\mathrm{K}$ the QHPs for $\nu = 2$ and $\nu = 4$ are clearly seen. The resistance values shown in Figure 4(d) and (e) are calculated with the same model, but for the smaller collision broadening parameter $\gamma = 0.05$.

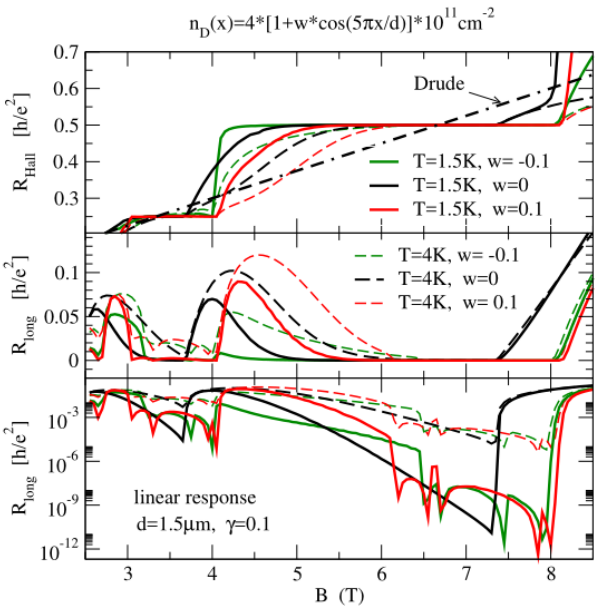


**Figure 8** Linear response result for the $B$-dependence of Hall resistance (upper panel) and longitudinal resistance (lower panels), defined in Eqs.(21) and (20), respectively. The middle panel shows $R_{\mathrm{long}}(B)$ on a linear scale and the lower panel on a logarithmic scale. The spatial average, Eq.(23), is performed with $\lambda = \ell_{\mathrm{B}} = \sqrt{10\mathrm{T}/B} \cdot 8.1\mathrm{nm}$. The Drude result $R_{\mathrm{Hall}} = h/(e^2 v_{eff})$ is also indicated for $w = 0$.

Apparently, the modulation extends the QHPs to higher $B$-values. This is immediately understood from Figure 5, since the maxima of the $n_{el}(x)$ curves for the modulated cases are larger than the maximum for the unmodulated case, and thus ISs with the same filling factor exist for the modulated cases at higher $B$-values than for the unmodulated case. Since above a critical $B$-value ($B \approx 8\mathrm{T}$ for $w = \pm 0.1$ and $B \approx 7.4\mathrm{T}$ for $w = 0$) no ISs exist, the high-$B$ edge of the ($\nu = 2$)-QHP is not sensitive to temperature. This is very different for the low-$B$ edge of this plateau, where ISs exist only near the sample edges. The width of an IS is inversely proportional to the slope $dn_{el}(x)/dx$ at its center, taken at $B = 0$ [14, 15]. According to Figure 5, near the edges, this slope is largest for $w = 0.1$, intermediate for $w = 0$ and smallest for $w = -0.1$, and at a given $B$, the ISs are narrowest, intermediate and widest, respectively. Therefore, the low-$B$ edge of the ($\nu = 2$)-QHP occurs for $w = 0.1$ at the highest and for $w = -0.1$ at the lowest $B$-value. At this low-$B$ value of the plateau, the increasing temperature destroys the quantization rapidly.

Of course, the width of a QHP depends not only on the lateral modulation of the donor density and on the temperature. The collision broadening of the Landau levels and the spatial averaging according to Eqs.(12) and (23) also affect the width of a calculated QHP, as has been discussed previously [27, 29, 38].

Near $B = 3.5\mathrm{T}$, Figure 8 indicates the existence of a ($\nu = 4$)-QHP for the cases with and without modulation, at least for $T = 1.5\mathrm{K}$. The quantization is, however, not well developed ($R_{\mathrm{long}}/R_{\mathrm{Hall}} \gtrsim 10^{-3}$) for $T = 1.5\mathrm{K}$, and does not exist for $T = 4\mathrm{K}$, whereas in the upper part of the ($\nu = 2$)-plateaus we find a good quantization with $R_{\mathrm{long}}/R_{\mathrm{Hall}} \ll 10^{-4}$, at least for the lower temperature $T = 1.5\mathrm{K}$. The cusp-structure seen in the logarithmic plot of $R_{\mathrm{long}}(B)$ (lowest panel of Figure 8) results from the fact, that the number of ISs in the system changes at these $B$-values. These results are consistent with those obtained for the modulation with $k_D = 1$ and $w = -1$ [40].

### *4.2 Temperature Dependence*

In the following section, we want to present the results of numerical calculations of electron and current density for different values of magnetic field, temperature, and strength of the ASDC, starting with weak currents, where we can expect results similar to the linear response regime. Similar calculations for the samples with homogeneous donor charge density can be found in the literature [27, 28, 38, 43]. We will consider here the modulation model introduced above, since it allows us to discuss the same physical concepts and some additional phenomena.

Before we start with the quantum calculation, we should remember the classical Drude model of magneto-transport, which describes, in the local version, longitudinal and Hall resistivities as

$$\rho_l(x) = 1/\sigma_0(x), \quad \rho_H(x) = \omega_c \tau \rho_l(x), \text{ (26)}$$

respectively, with $\sigma_0(x) = (e^2\tau/m)n_{el}(x)$ and a constant relaxation time $\tau$. According to Eqs.(17) this implies, that the current density is proportional to the electron density, $j_y(x) \propto n_{el}(x)$, and that the electrical field $E_x(x)$ is constant, i.e., $\mu^*(x)$ increases linearly with $x$.

Figure 9 shows results for $B = 6$T, where according to Figure 5 only two ISs near the sample edges are possible. The upper panels show current density $j_y(x)$ and filling factor $\nu(x) = 2\pi\ell_B^2 n_{el}(x)$, respectively, on a linear scale. Apparently for $T_L = 50$K the prediction of the Drude model is nicely satisfied: the current density $j_y(x)$ is proportional to the electron density $n_{el}(x)$ and the lowest panel shows the linear position-dependence of the electrochemical potential $\mu^*(x)$. This situation can be described by a constant scattering time $\tau$, i.e., a conductivity $\sigma_0(x)$ proportional to the electron density $n_{el}(x)$ or, at fixed $B$-field, proportional to the filling factor $\nu(x)$. This Drude behavior is consistent with the high-temperature behavior of our conductivity model, sketched Figure 7, since, for $B = 6$T and $T = 50$K, $t = k_B T/\hbar\omega_c = 0.415$.

This behavior changes, however, rapidly with a decreasing temperature. The overall shape of the density profiles changes very little with decreasing $T_L$, until for $T_L \lesssim 4$K two ISs develop near $x = \pm 0.72d$. Therefore the main plot of $\nu(x)$ shows only the curves for $T_L = 50$K and $T_L = 1.5$K, with insets showing the development of ISs. However, the current distribution $j_y(x)$ changes its shape drastically. At $x \approx \pm 0.72d$, where the local filling factor becomes two, $\nu(x) = 2$, according to Eqs.(22) and Figure 7 the longitudinal conductivity $\sigma_l(x)$, and thus the longitudinal resistivity $\rho_l(x)$, decrease with decreasing temperature and become exponentially small for $t = k_B T/\hbar\omega_c \ll 1$. According to Eq.(17), then $j_y(x)$ becomes very large at these positions, and very small elsewhere, since the total ASDC $I$ is kept constant. The strong changes of the current distribution with decreasing temperature are clearly seen in the linear and the logarithmic plot of $j_y(x)$ in Figure 9. The lowest two panels of the figure also show that even for this small ASDC of $I = 0.05\mu$A, the current distribution becomes very asymmetric at very low temperatures, here at $T_L \lesssim 2$K. At these low temperatures, essentially all the ASDC flows through the edge-near ISs at $x = \pm 0.72d$, in which the intrinsic edge-currents flow due to the finite gradient of the confinement potential. The intrinsic Hall current near $x = 0.72d$ has the same direction as the ASDC, the intrinsic current near $x = -0.72d$ has the opposite direction. As a result, the induced current in the IS near $x = 0.72d$ is stronger and leads to a larger increase in the Hall potential than the induced current on the opposite side of the sample.

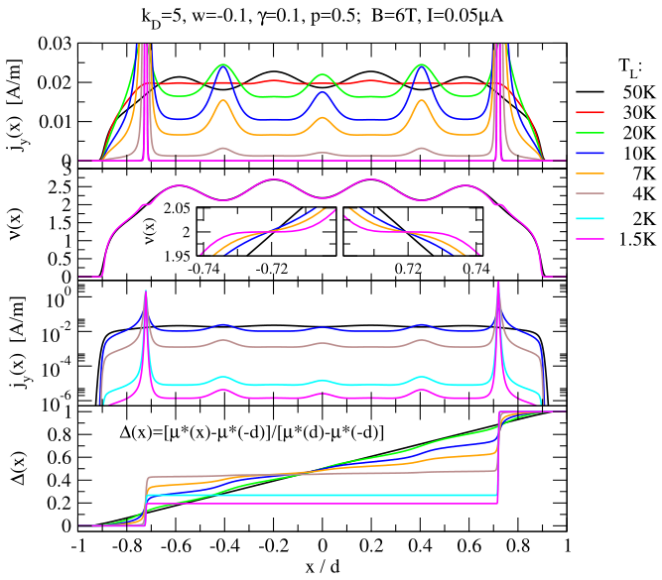


**Figure 9** Current density (uppermost and third panel), local filling factor (second panel) and normalized electrochemical potential $\mu^*(x)$ (lowest panel) for the indicated lattice temperatures. The insets of the $\nu(x)$-plot show the regions around the ISs near $x = \pm 0.72d$ for several $T$-values.

Here the situation of the IQHE is approached continuously by lowering the temperature, which leads to stripes, in which $\nu(x)$ approaches the value two, so that the local longitudunal resistivity $\rho_l(x)$ becomes small (Shubnikov-deHaas effect). Since in a stationary non-equilibrium state, the entropy production should be minimal, the current density occupies the regions with minimal $\rho_l(x)$ and thus minimizes the dissipation. If the ISs are so well developed, that all the ASDC can flow through stripes with $\nu(x) = 2$, the sample shows the IQHE.

So far the discussion applies to modulated systems at the lower part of a QHP and to unmodulated systems, where in the situation of the IQHE, the current is restricted to two ISs. In the modulated systems, some additional effects may occur. There may be more than two ISs with the same integer filling factor, as we will discuss below. In the case considered in Figure 9 the filling factor $\nu(x)$ has three local minima near $x = \pm 0.4d$ and in the center at $x = 0$, where $\nu(x)$ is only slightly larger than two. With the decreasing temperature ($T_L \lesssim 20\text{K}$) at these positions relative minima of $\rho_l(x)$ and relative maxima of $j_y(x)$ occur. These relative maxima become, however, irrelevant at low temperature, $T_L < 4\text{K}$, where the IQHE occurs.

Since the ASDC is rather small, Joule heating, and therefore the local increase of the electron temperature, is rather small at high and at very low lattice temperatures. At intermediate temperatures, $4\text{K} \lesssim T_L \lesssim 10\text{K}$, the current density $j_y(x)$ is already enlarged in the regions, where ISs start to develop. In these regions is, however, $\rho_l(x)$ still relatively large, so that Joule heating in these regions leads to $T_{el}(x)$ a few per cent larger than $T_L$. This heating effect is considered in the calculation ($p = 0.5$), but since it is rather small, we do not discuss it here.

In Figure 10 we consider the results for $B = 7\text{T}$ and the modulation model of Eq.(13) for $k_D = 5$ and $w = 0.1$ (left panels) and $w = -0.1$ (right panels). Here the ASDC is twice as large as in Figure 9, but the assumed Joule heating is much smaller ($p = 0.1$). For homogeneous donor density one would again expect that two ISs develop at low temperature, which then carry all the ASDC, but now up to eight ISs are possible. As in Figure 9, the position dependence of current density, filling

factor, and normalized electrochemical potential is shown. For high temperatures, $j_y(x)$ is plotted on a linear scale (uppermost panels) and for low temperatures on a logarithmic one (third panels from above). Since the $\nu(x)$-curves for all considered temperatures would fall very close together, we show them only for $T_L = 50\text{K}$ and $T_L = 1.5\text{K}$. Again the results for $T_L = 50\text{K}$ are in good agreement with the predictions of the Drude model. However, already for $T_L = 30\text{K}$, the structures of the $j_y(x)$-profiles are rather different from the corresponding $\nu(x)$-profiles, which are nearly identical with the $\nu(x)$-profiles for $T_L = 50\text{K}$. Further, already at rather high temperatures, for $T_L \lesssim 20\text{K}$, the density of the ASDC starts to concentrate on the regions, where the local filling factor is close to two, $\nu(x) \approx 2$, and $\rho_l(x)$ becomes small with the decreasing temperature, and where at a low temperature, $T_L \lesssim 2\text{K}$, the ISs develop and carry the current nearly dissipationless. Figure 10 shows clearly, that, in the modulated system, for magnetic fields in the upper part of the QHP, the current distribution extends over a wide region of the Hall bar ("bulk-dominated regime"), whereas the unmodulated system, at this $B$-value, would develop two ISs near $x = \pm 0.5d$, which would carry all the current. The lower panels of Figure 10 show clearly that the ISs are not equivalent. Some of the ISs carry more current than others, and at very low $T_L$, a single IS starts to dominate. Here, two aspects are relevant for the current transport in an IS. As we have already discussed, the IS can carry more of the ASDC, if its intrinsic current has the same direction as the ASDC. Another aspect is the width of the IS. If, at higher $T_L$, the density gradient at the center of the IS, where $\nu(x) = 2$, is small, the resulting IS will have a larger width than if this gradient is large [14]. Since wider ISs can carry more current than narrow ISs, those ISs, which evolve at positions with a small density gradient and have an intrinsic Hall current with the direction of the ASDC, are most favorable for the transport of the ASDC. This explains the low-temperature results of Figure 10. Again the effect of Joule heating is rather small and we do not discuss it here in detail.

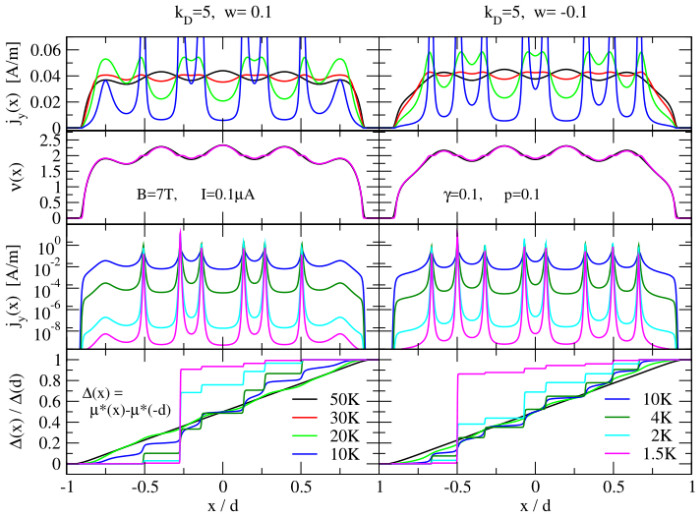


**Figure 10** Current density, filling factor, and normalized electrochemical potential across the Hall bar, as in Figure 9, but for $B = 7\text{T}$, $I = 0.1\mu\text{A}$ and the modulation models of Eq.(13) with $k_D = 5$ and $w = \pm 0.1$.

Another example of the peculiar interaction of temperature, Joule heating and current strength is given in Figure 11 for the donor density modulation model with $k_D = 1, w = -0.1$. The left panels compare the effective confinement energy $U(x)$, the lowest Landau bands $\varepsilon_n(x) = U(x) +$

$\hbar\omega_c(n+1/2)$ and the electrochemical potential $\mu^*(x)$ with ASDC, $I = 0.6\mu$A (black lines), and without, $I = 0$ (red lines), at $B = 6.7$T and $T_L = 2$K. The confinement energies $U(x)$ at $T_L = 50$K are also indicated for comparison, which show much less structure than the corresponding quantities at $T_L = 2$K. At $T_L = 2$K and $I = 0$ the electron density has the symmetry $n_{el}(-x) = n_{el}(x)$ and develops two ISs near $x = \pm 0.3d$, which are considerably broader than those near $x = \pm 0.7d$, because the slope $dn_{el}(x)/dx$ at $x = \pm 0.3d$ is not so steep as at $x = \pm 0.7d$ [14, 15].

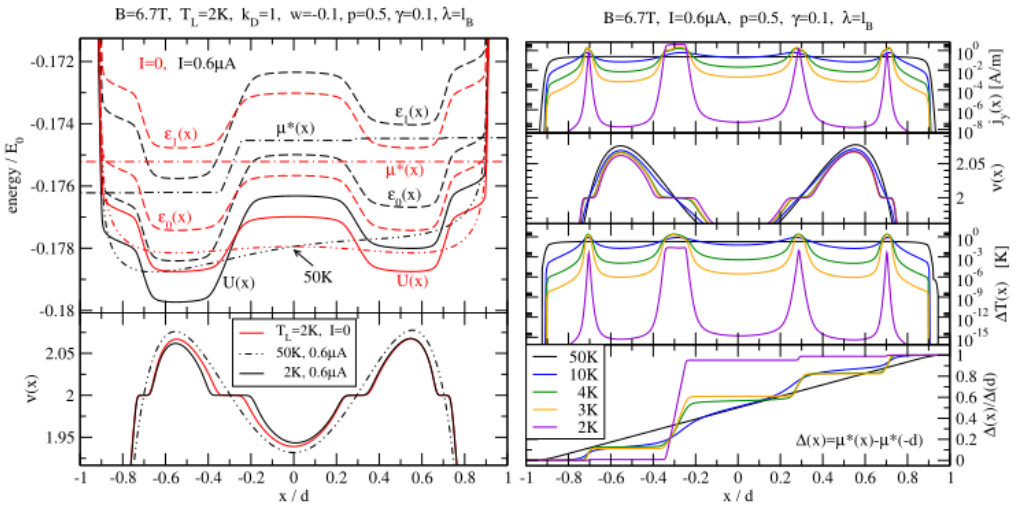


**Figure 11** Left panels: Effective confinement energy $U(x)$, Landau bands $\varepsilon_n(x)$ and electrochemical potential $\mu^*(x)$ (upper panel) and resulting filling factor (lower panel) at $T_L = 2$K without (red) and with (black) ASDC $0.6\mu$A. Right panels: density of ASDC, filling factor, $\Delta T(x) = T_{el}(x) - T_L$ and normalized electrochemical potential for $B = 6.7$T, $I = 0.6\mu$A and the indicated lattice temperatures.

The ASDC destroys this symmetry and broadens considerably the IS near $x = -0.3d$, where the intrinsic current has the same direction as the applied one. This current-induced asymmetry is also seen in the right panels of Figure 11, which show, from top to bottom, the current density, the filling factor, the enhancement of the electron temperature due to Joule heating and the normalized electrochemical potential as functions of the position $x$. These plots also demonstrate the strong effect of the lattice temperature. With decreasing $T_L$ the current density $j_y(x)$, here plotted in a logarithmic scale, is more and more confined to the regions, where the ISs will appear at sufficiently low temperature. In the figure this starts at about $T_L = 10$K and a confinement of comparable amounts of current on the four regions near $x = \pm 0.3d$ and $x = \pm 0.7d$ is seen down to $T_L = 3$K. In this regime the longitudinal resistivity is still so large, that Joule heating increases the local electron temperature considerably, $\Delta T(x) \sim 2.5$K, in the IS-regions for $T_L = 3$K and 4K, but only $\Delta T(x) \lesssim 0.2$K for $T_L = 50$K. This changes drastically as $T_L$ is lowered further. At $T_L = 2$K the conductivity components $\rho_l(x)$ and $\rho_H(x)$ in the broad IS near $x = -0.3d$ are well quantized, most of the ASDC flows with nearly constant current density $j_y(x)$ and constant Hall field $E_x(x) = e^{-1}\partial\mu^*(x)/\partial x$ through this stripe and the increase of the local electron temperature is very small, $\Delta T(x) \leq 0.03$K, by orders of magnitude smaller than at $T_L = 3$K [40]. These drastic changes with temperature will, of course, lead to strong variations of the global resistance components, which will be discussed in the following sections. For the situations discussed here, we find, for instance,

$(e^2/h)R_{\mathrm{long}} \approx 1.1 \cdot 10^{-4}$ and $(e^2/h)R_{\mathrm{Hall}} - 0.5 \approx 6 \cdot 10^{-5}$ at $T_L = 3\mathrm{K}$, but $(e^2/h)R_{\mathrm{long}} \approx 2.4 \cdot 10^{-9}$ and $(e^2/h)R_{\mathrm{Hall}} - 0.5 \approx 2 \cdot 10^{-8}$ at $T_L = 2\mathrm{K}$.

Another interesting effect is demonstrated by the upper left panel of Figure 11. Due to the applied current, near $x = -0.3d$ states of different Landau bands have the same energy, $\varepsilon_1(x_1) = \varepsilon_0(x_0)$ for $x_1 < x_0$. With increasing current $I$, the distance $x_0 - x_1$ will decrease. If this distance approaches the extent of the corresponding eigenfunctions, which is of the order of the magnetic length $\ell_B$, impurity or phonon mediated quasi-elastic inter-Landau-level scattering (QUILLS) may become possible, which has been discussed as a possible breakdown mechanism of the IQHE [21, 47].

### *4.3 Effect of Current Strength and Joule Heating*

For the models considered here, the reflection symmetry $n_{el}(-x) = n_{el}(x)$ holds in the absence of an ASDC and in the linear response limit, but is destroyed by a finite applied current. This was already indicated in the early experiments [12] and clearly seen in the first calculation, trying to explain these experiments [28]. Later this current-induced asymmetry of the current-density was investigated systematically, both experimentally [39, 45] and theoretically [38, 43].

The strong asymmetry caused by increasing strength of the ASDC is nicely demonstrated in Figure 12, which is obtained for homogeneous donor density and neglecting Joule heating [38, 43]. For very weak current, in the linear response regime (black lines), at temperature $T = 4\mathrm{K}$, two symmetric ISs with local filling factor $\nu(x) = 2$ occur near $x = \pm 0.525d$. Both of them carry a half of the ASDC that is nearly dissipation−less. Since nearly all current flows through these stripes, the Hall potential increases in two equally high steps across these stripes. With increasing current−strength, the IS near $x = 0.525d$, in which the intrinsic current has the same direction as the ASDC, becomes wider and carries a larger part of the ASDC, while the IS near $x = -0.525d$ shrinks a little and carries a decreasing part of the current. As a consequence, the step of the Hall potential near $x = -0.525d$ becomes smaller than that near $x = 0.525d$. In this calculation, which neglects Joule heating, the main effect of the increasing current-strength is to broaden one of the stripes and to concentrate most of the current on this stripe.

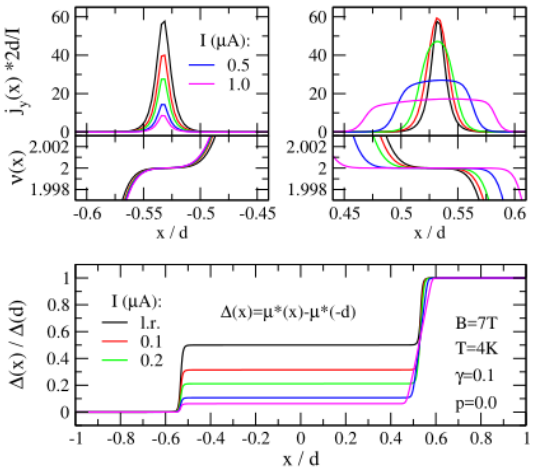


**Figure 12** Current-induced asymmetry of the normalized Hall potential (lower panel) and of current-carrying ISs (medium panels) and the current density (upper panels). Joule heating is neglected ($p = 0$), $\lambda = \ell_B$, homogeneous donor density.

Consideration of Joule heating, as in Figure 13 for $p = 0.5$, changes things considerably. Now the current-induced asymmetry is less pronounced and for a larger strength of the ASDC an increasing part of this current spreads out from the ISs into the dissipative bulk, leading to a breakdown of the IQHE. This is similar to the experimental finding that the longitudinal resistance increases continuously with increasing current-strength from nearly zero in the quantum Hall regime at small currents to the normal dissipative regime at strong currents. According to Figure 13, for $p = 0.5$, the IQHE breaks down for $I \gtrsim 0.2\mu$A: there exist no longer ISs with constant filling factor and the Hall potential takes on a finite slope in the bulk. If the thermal contact between the 2DES and the host lattice is better, so that the Joule heating of the 2DES is weaker, these effects are less pronounced. For $p = 0.1$ the breakdown of the IQHE sets in only for $I > 0.5\mu$A, but the asymmetry of the current distribution is already much smaller than for $p = 0$ [43].

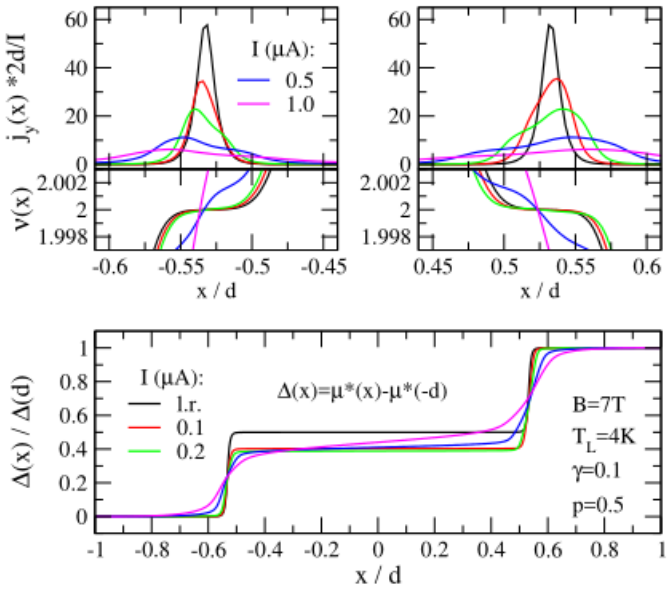


**Figure 13** Same as Figure 12, but under consideration of Joule heating, $p = 0.5$.

The reason for this breakdown of the QHE is, of course, the local increase of the electron temperature in the stripes, where most of the ASDC flows. This local increase of $T_{el}(x)$ depends on the strength of the heat transfer to the lattice and is shown in the upper panels of Figure 14 for a stronger ($p = 0.1$) and a weaker ($p = 0.5$) heat transfer.

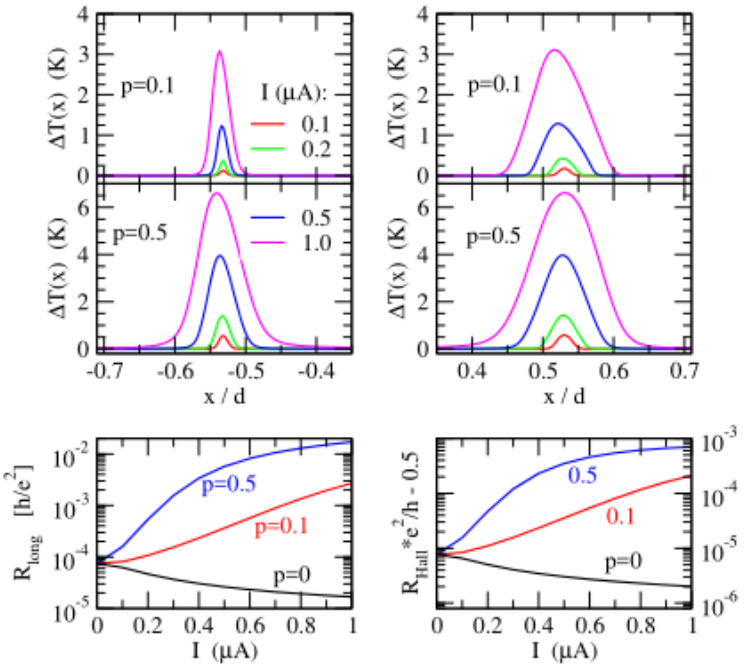


**Figure 14** Upper panels: the increase in electron temperature, $\Delta T(x) = T_{el}(x) - T_L$, due to Joule heating (for $p = 0.1$ and $p = 0.5$) for the indicated values of the ASDC $I$. Lower panels: longitudinal resistance $R_{\mathrm{long}} = \frac{2dE_y^0}{I}$ and Hall resistance $R_{\mathrm{Hall}} = [\,\mu^*(d) - \mu^*(-d)]/(eI)$ versus applied current $I$ without ($p = 0$) and with ($p = 0.1$ and $p = 0.5$) Joule heating. All panels are for $B = 7\mathrm{T}$, $T_L = 4\mathrm{K}$ and for $\gamma = 0.1$ and $\lambda = \ell_B$ as in Figures 12 and 13.

The lower panels of the figure show the longitudinal and the Hall resistance as a function of the applied current without and with consideration of Joule heating, for a sample with the same parameters as in Figures 12 and 13. Without Joule heating ($p = 0$), the resistances come with increasing ASDC closer to the quantized values $R_{\mathrm{long}} = 0$ and $R_{\mathrm{Hall}} = 0.5h/e^2$. With Joule heating, on the other hand, the resistances deviate with increasing $I$ increasingly from the quantized values, so that an increasing applied current can cause a continuous breakdown of the quantized situation. This is the result for the lattice temperature $T_L = 4\mathrm{K}$. At lower $T_L$, the Joule heating will, however, lead to a much more complicated situation, as is demonstrated in Figure 15 [43]. The upper panels in Figure 15 show that, in the absence of Joule heating, for the considered model with homogeneous donor charge, at $B = 7\mathrm{T}$, the situation of the IQHE is reached for $T_L \lesssim 4\mathrm{K}$. Increasing the ASDC $I$ changes the resistance values only a little, and slightly improves the quantization conditions, in agreement with the result of Figure 14. Since the curves for $I \geq 0.5\mu\mathrm{A}$ are very close to each other, only a few of them are shown.

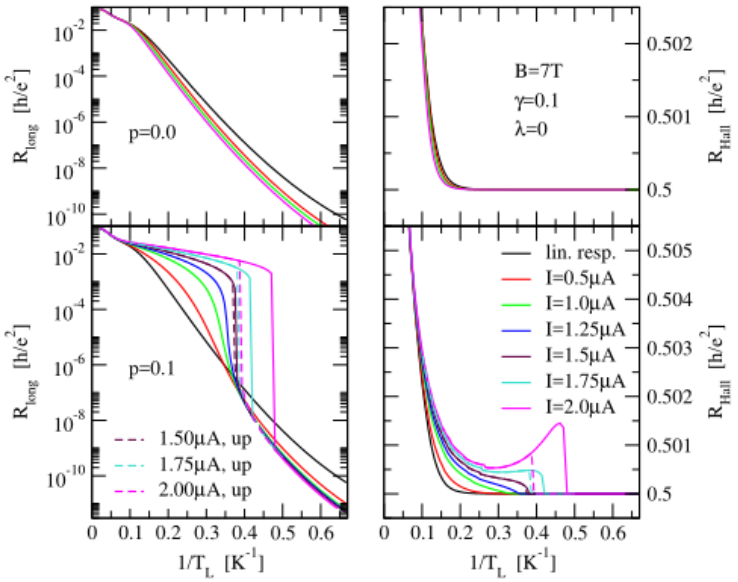


**Figure 15** Longitudinal resistance $R_{\rm long} = \frac{2dE_y^0}{I}$ (left panels) and Hall resistance $R_{\rm Hall} = [\,\mu^*(d) - \mu^*(-d)]/(eI)$ (right panels) as functions of the inverse lattice temperature $T_L$ for $1.5{\rm K} < T_L < 50{\rm K}$ and for several values of the applied current $I$. The upper panels show results without ($p = 0$) and the lower panels results with ($p = 0.1$) Joule heating. In the lower panels the $T_L$-dependence shows a hysteresis for $I \gtrsim 1.5\mu$A.

If Joule heating is considered, similar results hold only for very low lattice temperatures and not too large ASDCs, e.g., for $T_L \lesssim 2{\rm K}$ and $I \lesssim 2\mu$A in Figure 15 ($p = 0.1$). At higher temperatures ($T_L \gtrsim 3{\rm K}$) one finds the behavior seen in Figure 14 for $p > 0$: the longitudinal resistance increases with increasing current and a continuous breakdown of the QHE occurs, if it exists at small $I$. At lower temperatures ($T_L \lesssim 2.8{\rm K}$), the situation becomes different. As $I$ increases towards $1.5\mu$A, the slopes of the $R_{\rm long}(1/T_L)$-curves become very steep, and for $I > 1.5\mu$A these curves become discontinuous at a temperature $T_L = T_{cr}(I)$, which decreases with increasing $I$. If an ASDC $I > 1.5\mu$A is fixed and the temperature is lowered (from $T_L = 50{\rm K}$) towards $T_{cr}(I)$, the 2DES is in a normal dissipative state and its longitudinal resistance decreases slightly with decreasing $T_L$. If the temperature is lowered further, the 2DES undergoes an abrupt transition to a quantum Hall state. For $T_L < T_{cr}(I)$, the ASDC flows nearly dissipationless through ISs and $R_{\rm long}$ and $R_{\rm Hall} = h/(ie^2)$ are many orders of magnitude smaller than $h/e^2$, and decrease further with decreasing $T_L$. In this regime larger currents result, at fixed $T_L$, in smaller values of $R_{\rm long}$, i.e., Joule heating plays no role. The abrupt transition from a dissipative state at higher $T_L$ to a quantum-Hall state at lower $T_L$ introduces a hysteresis. If one fixes $I > 1.5\mu$A and increases $T_L$, starting from a value less than $T_{cr}(I)$, one remains in the quantized state until one reaches an upper critical temperature $T_{cr}^{up}(I) > T_{cr}(I)$.

For $T_L > T_{cr}^{up}(I)$ the 2DES is again in the dissipative "high temperature state". The dashed lines in Figure 15 show the resistances obtained during this increase of $T_L$. In the interval $T_{cr}(I) < T_L < T_{cr}^{up}(I)$, two states, namely, a dissipative and a quantum-Hall state, coexist and it depends on boundary conditions and on the history of the experiment, in which of these states, the system is found.

The calculations for Figure 15 have been performed without modulation of the donor charge-density and without a spatial average of electron density and conductivity. Calculations with such spatial averages and without modulation as well as with modulation [40] of the donor density have also been performed and yielded qualitatively very similar results. In Figure 15 a $B$-value in the high-$B$ region of the $(\nu = 2)$-QHP is considered, and therefore $R_{\mathrm{Hall}}$ in the not-quantized dissipative states is larger than $0.5h/e^2$ (see e.g., Figure 8). For a $B$-value in the low-$B$ region of the QHP, one gets in the dissipative states, the values $R_{\mathrm{Hall}} < 0.5h/e^2$ [40, 43], as is shown in Figure 16, which was calculated under due consideration of Joule heating and spatial averaging.

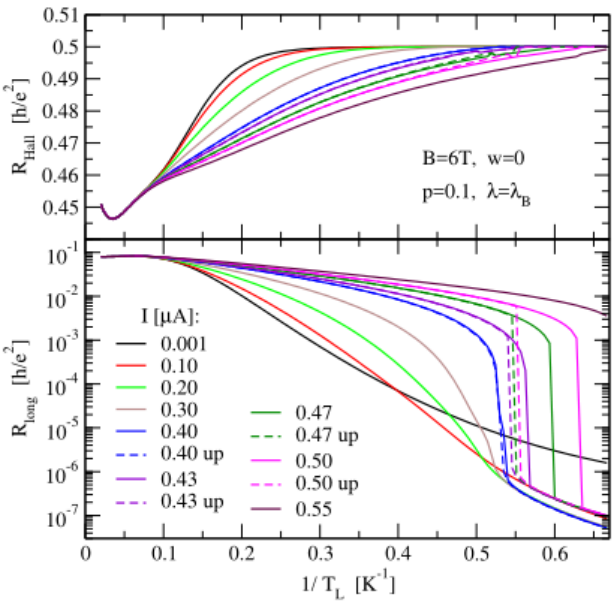


**Figure 16** Hall resistance $R_{\mathrm{Hall}} = [\mu^*(d) - \mu^*(-d)]/(eI)$ and longitudinal resistance $R_{\mathrm{long}} = \frac{2dE_y^0}{I}$ versus inverse lattice temperature for $B = 6\mathrm{T}$ and different applied currents, with Joule heating $(p = 0.1)$ and spatial avering $(\lambda = \ell_B)$; other parameters as in Figure 15. Dashes lines are for increasing $T_L$.

### *4.4 Current-Driven Breakdown*

In the previous section 4.3 we have seen, that the strength of an ASDC strongly affects the temperature dependence of longitudinal and Hall resistance. So it should be interesting to calculate these resistances at fixed lattice temperature as a function of the applied current, and to compare the result with experimental data. Such experiments have been published in figure 3 of [39], where a "longitudinal voltage", proportional to the longitudinal resistance, was measured as a function of a bias voltage, which determined the applied current.

The results for the $(\nu = 2)$-QHP can be summarized as follows. The resistance increases with increasing current, so that a continuous breakdown of the QHE is observed. As $B$ is lowered from the center of the QHP towards its lower edge, for a smaller $B$ the breakdown sets in at a smaller current and the slope of the function $R_{\mathrm{long}}(I)$ becomes steeper. As $B$ is increased from the center towards the high-$B$ edge of the QHP, for larger $B$, the breakdown sets in at a smaller $I$ and the slope of $R_{\mathrm{long}}(I)$ increases with increasing $B$. In general, these slopes are steeper for $B$ in the high-$B$ part of the QHP than for $B$ in its low-$B$ part.

The calculated results for the unmodulated model ($w = 0$) at the relatively high temperature $T_L = 2.5$K are shown in Figure 17. For these parameters the ($\nu = 2$)-QHP is located at 6T$\lesssim B \lesssim$ 7.35T and the medium panel of the figure shows, that for the lower part of the QHP (6T$\leq B \leq$ 6.7T) the $I$-dependence of $R_{\rm long}$ is in qualitative agreement with the mentioned experiment (figure 3 of a previous paper [39]). This is easily understood since the ISs become smaller with decreasing $B$ and even in the breakdown regime the current is concentrated on a narrower stripe than at larger $B$-values. Therefore, at lower $B$ the same current $I$ leads to a higher current density and a stronger effect of Joule heating and, as a consequence, to a larger resistance. This explains the observed breakdown-behavior in the low-$B$ part of the QHP. The logarithmic plot in the lowest panel of Figure 17 gives some additional information about the quantized situation, where $R_{\rm long} \lesssim 10^{-4} h/e^2$. There, for small $I$, $R_{\rm long}(I)$ first decreases with increasing $I$, because Joule heating is not yet effective and increasing $I$ just broadens one of the ISs. But at larger $I$, when Joule heating becomes effective, the increase of $R_{\rm long}(I)$ with $I$ becomes steeper with increasing $B$ and apparently becomes discontinuous for $B > 6.7$T. The Newton-Raphson iteration procedure, used to calculate the data of Figure 17, was not able to describe these discontinuities, probably because it relies on successive small changes of the thermodynamic state of the system. Similar calculations for lower temperature, $T_L = 1.5$K, and slightly other parameters for Joule heating and spatial averaging, led to similar results, although at somewhat smaller values of $B$ and $I$, as shown in figure 9 of a previous paper [43].

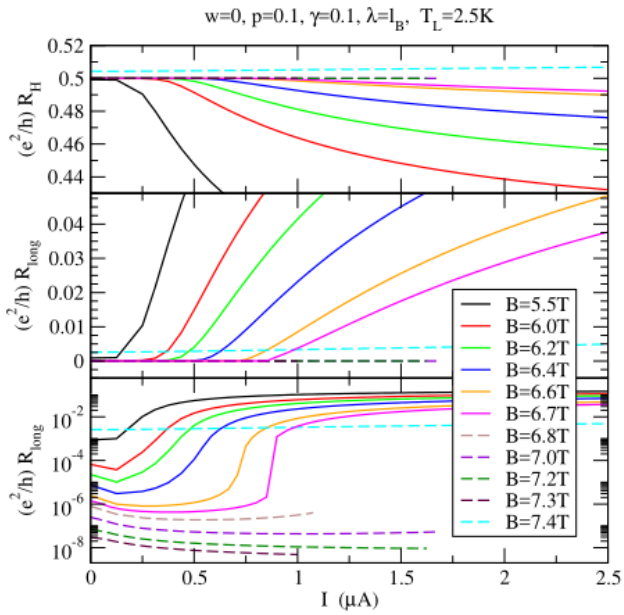


**Figure 17** Hall resistance (upper panel) and longitudinal resistance in linear (medium) and logarithmic scale (lower panel) versus ASDC $I$ for the model with unmodulated donor charge ($w = 0$) at $T_L = 2.5$K; with Joule heating ($p = 0.1$) and spatial averaging ($\lambda = \ell_B$).

Convergent result for all $B$-values in the ($\nu = 2$)-QHP are obtained for a model with modulated donor density (Eq.(13) with $k_D = 1$, $w = -0.1$), at least for the relatively high temperature $T_L = 2.5$K, as shown in Figure 18 (compare figure 7 of the earlier study [40]). The linear plot of $R_{\rm long}(I)$ (lowest panel) shows for $B$-values in the lower part of the QHP, i.e. for 6.4T $\lesssim B \lesssim$ 6.8T,

similar behavior as the middle panel of Figure 17: with decreasing $B$ the breakdown of the quantized situation sets in at lower values of $I$ and the slope of the $R_{\mathrm{long}}(I)$-curves in the dissipative regime becomes steeper. The behavior of the $R_{\mathrm{long}}(I)$-curves in the upper part of the QHP ($6.90\mathrm{T} \lesssim B \lesssim 6.93\mathrm{T}$) is different: with increasing $B$ the breakdown sets in at a smaller $I$-value, and, in the dissipative regime, the slope of the $R_{\mathrm{long}}(I)$-curves increases with increasing $B$ as in the mentioned experiments. However, in contrast to the experimental results, in the upper part of the QHP, the slopes of the $R_{\mathrm{long}}(I)$-curves are much smaller than in the low-$B$ part. The reason for this discrepancy is probably the simple – and unrealistic – modulation model, which leads to maxima of the electron density near $x = \pm 0.52d$, which determine the position of the ISs for $B$-values in the upper part of the QHP (see Figure 5).

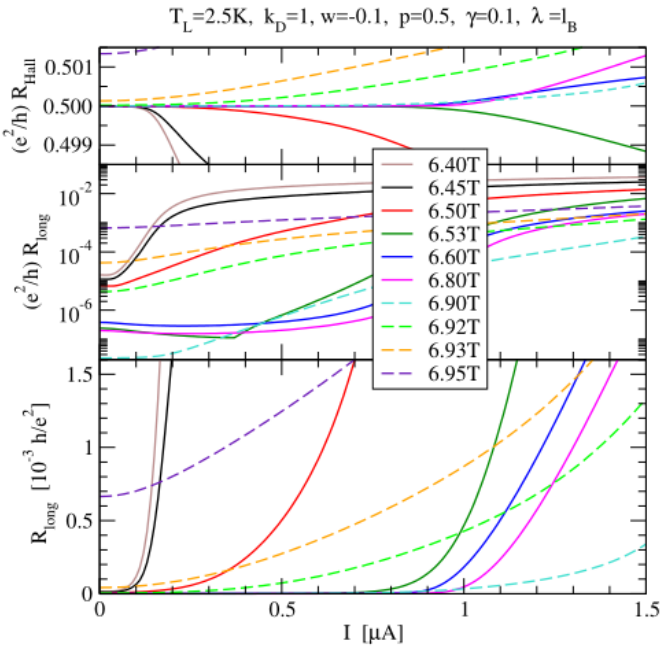


**Figure 18** Hall resistance (upper panel) and longitudinal resistance on logarithmic (middle panel) and linear scale (lower panel) versus ASDC $I$ for a modulated sample ($k_D = 1, w = -0.1$) at temperature $T_L = 2.5\mathrm{K}$. Joule heating, collision broadening, and spatial averaging are considered.

At lower lattice temperature also this modulation model leads to convergence problems of the Newton-Raphson iteration [40]. At $T_L = 1.5\mathrm{K}$ the QHP, at $6.0\mathrm{T} \lesssim B \lesssim 6.92\mathrm{T}$, extends to lower $B$-values than at $T_L = 2.5\mathrm{K}$, due to the existence of ISs near the sample edges. In the low-$B$ range $6.0\mathrm{T} \lesssim B \lesssim 6.45\mathrm{T}$, where only these edge-near ISs exist, the behavior of the $R_{\mathrm{long}}(I)$-curves is similar to those in the unmodulated case (Figure 17): for small $I$, $R_{\mathrm{long}}(I)$ first decreases with increasing $I$, as long as Joule heating is ineffective, and then suddenly increases at larger $B$ eventually with a discontinuous breakdown of the quantized state, which leads to the mentioned convergence problems. Only close to the high-$B$ edge of the QHP, for $6.90\mathrm{T} \lesssim B \lesssim 6.92\mathrm{T}$, a continuous increase in $R_{\mathrm{long}}(I)$ from a quantized situation at low $I$ to a dissipative situation at high $I$ could be calculated (see figure 9 of [40]). In the quantized regime, the interesting structures in the $R_{\mathrm{long}}(I)$-curves occur for $B$-values, for which the current flows through different ISs located close to a relative extremum of the electron density profile $n_{el}(x)$. Then increasing current

strength $I$ may change the current distribution among these stripes and change their shapes, and may even force them to merge to a single incompressible region (see figures 9 and 10 of the article [40]).

If for a QHP the number of available ISs changes with changing magnetic field, the structure of the corresponding $R_{\mathrm{long}}(I)$-curves may also change. An example is given in Figure 19 for the modulation model of Eq.(13) with $k_D = 5$ and $w = 0.1$. At lattice temperature $T_L = 2\mathrm{K}$ the $(\nu = 2)$-QHP extends from $B \approx 6.1\mathrm{T}$ to $B \approx 8.1\mathrm{T}$. For $B \lesssim 6.0\mathrm{T}$ the current density is concentrated on two edge-near stripes, which may become incompressible and carry the current dissipationless at lower temperatures. In the low-$B$ region of the QHP, for $6.0\mathrm{T} \lesssim B \lesssim 6.2\mathrm{T}$, where six ISs exist, a more or less continuous breakdown of the quantized situation is observed, similar to that in an unmodulated sample. In the interval $6.4\mathrm{T} \lesssim B \lesssim 8.0\mathrm{T}$, where number and position of the possible ISs change, the logarithmic plot of $R_{\mathrm{long}}(I)$ indicates several discontinuities and convergence problems of the Newton-Raphson iteration. At the high-$B$ end of the QHP, for $B = 8.1\mathrm{T}$, one observes again a continuous increase of $R_{\mathrm{long}}(I)$ from a quantized state at very low $I$ to dissipative states at larger $I$.

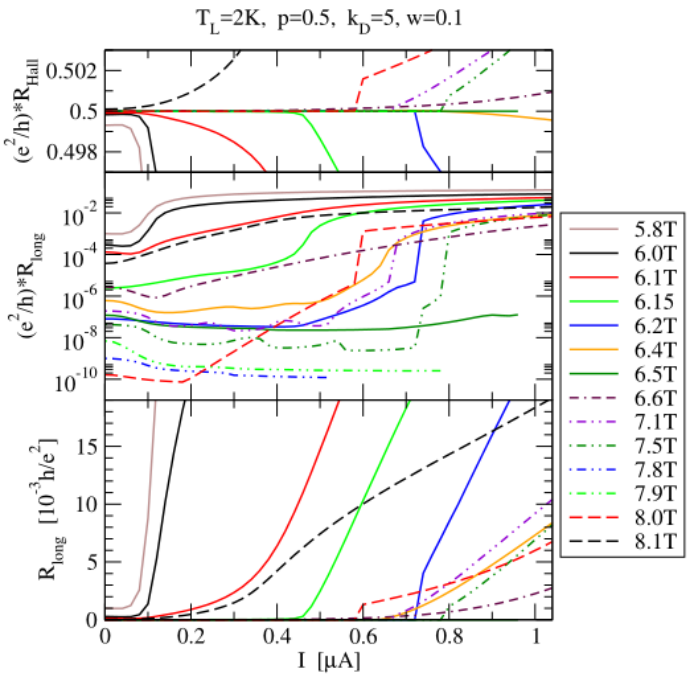


**Figure 19** Hall resistance (upper panel) and longitudinal resistance on logarithmic (middle panel) and linear scale (lower panel) as a function of the ASDC for the modulated model with $k_D = 5$ and $w = 0.1$ at lattice temperature $T_L = 2\mathrm{K}$, with Joule heating ($p = 0.5$) and spatial averaging ($\lambda = \ell_B$).

### *4.5 Dependence of Current Distribution on Lattice Temperature and Joule Heating*

The distribution of the imposed current among the available incompressible stripes depends sensitively on several parameters, such as lattice temperature $T_L$, strength $I$ of the current, and the effectiveness of Joule heating, modeled by the parameter $p$. The current density $j_y(x)$ in ISs is proportional to the gradient of the Hall potential, and its spatial distribution is easily read off from the position dependence of the normalized Hall potential $H(x;I) = \Delta(x)/\Delta(d)$, where $\Delta(x) =$

$\mu^{\star}(x) - \mu^{\star}(-d)$. Since in the absence of imposed current, our model has the inversion symmetry $n_{\mathrm{el}}(-x) = n_{\mathrm{el}}(x)$, the inversion of the current direction leads to $H(x;-I) = 1 - H(-x;I)$, and in the linear response limit of weak imposed current, $I \to 0$, the symmetry $H(x;-I) = H(x;I)$, and consequently $H(-x, I \to 0) = 1 - H(x, I \to 0)$, must hold. In the following we show, how $H(x;I)$ changes with the above mentioned parameters.

Figure 20 shows $H(x;I)$ for several values of $I$ and two values of the magnetic field at lattice temperature $T_L = 4\mathrm{K}$. In the upper panels Joule heating is neglected, $p = 0$, and in the lower panels it is assumed to be weak, $p = 0.1$. The upper panels show that with increasing $I$ the symmetry $H(x;I) = 1 - H(-x;I)$ is rapidly destroyed [46]. For larger $I$, most of the imposed current, which for small $I$ is more or less homogeneously distributed over the available stripes with $\nu(x) \approx 2$, flows through a single IS, which is located in the deepest minimum of the self-consistent effective potential and has an intrinsic Hall current in the direction of $I$. This is in agreement with the results of Figures 9 and 10. But these results are drastically changed due to Joule heating, which turns out to be important at this relatively high lattice temperature of $T_L = 4\mathrm{K}$. The lower panels of Figure 20 show that, due to Joule heating, for $B = 7.33\mathrm{T}$, i.e., closely below the high-$B$ edge of the ($\nu = 2$)-QHP, the imposed current is nearly equally distributed over the available stripes with $\nu(x) \approx 2$, indicating a higher effective electron temperature than $T_L$. For $B = 6\,\mathrm{T}$ near the low-$B$ edge of the plateau, Joule heating leads to a leaking of the imposed current out of the ISs near the sample edges into the bulk, and the finite slope of $H(x;I)$ in the bulk region indicates the current-induced breakdown of the QHE.

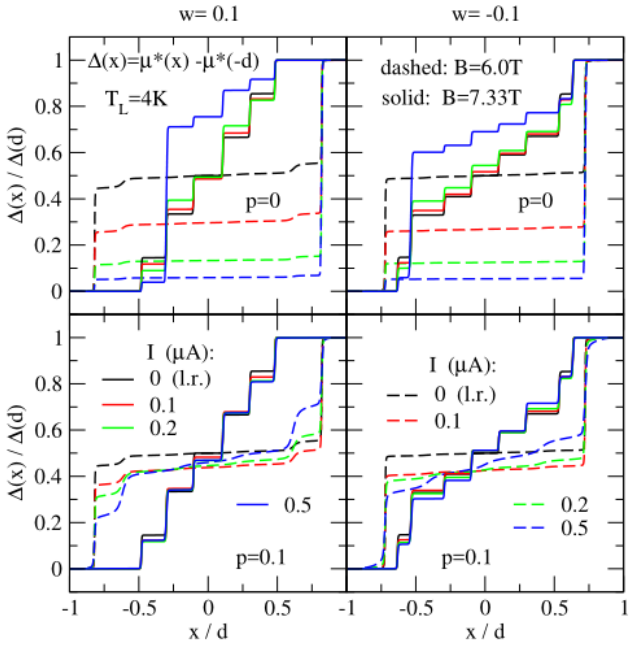


**Figure 20** Position dependence of the normalized Hall potential in Hall bars with modulated donor charge density, Eq.(13) with $k_D = 5$ and $w = 0.1$ (left panels) and $w = -0.1$ (right panels). Joule heating is neglected ($p = 0$) in the upper panels and weak ($p = 0.1$) in the lower panels. Solid lines refer to $B = 7.33T$, dashed lines to $B = 6T$, for different currents $I$ as indicated. $T_L = 4K$, $\gamma = 0.1$, $\lambda = \ell_B$.

The results of Figure 20 show that Joule heating counteracts the current-induced asymmetry of current distribution and Hall potential. Since the longitudinal conductivity in the ISs, and therefore the dissipation, becomes smaller with decreasing temperature, we expect that with decreasing $T_L$ the effect of Joule heating becomes less important. This is indeed shown by Figure 21, which considers Joule heating with $p = 0.5$, which in principle is more efficient than $p = 0.1$. The results for $T_L = 4\,\mathrm{K}$ (upper panels) are very similar to those of Figure 20 for $p = 0.1$ and $B = 7.33\mathrm{T}$: due to the Joule heating, the current-induced asymmetry is largely suppressed, the Hall potential profiles are nearly independent of the strength of the imposed current and close to the linear response limit. For $T_L = 1.5\mathrm{K}$ (lowest panels) and $T_L = 2\mathrm{K}$ (medium panels), on the other hand, the imposed current leads to strong asymmetries, which do, however, not evolve in a continuous manner with increasing $I$. For $0 < I \leq 0.2\,\mu\mathrm{A}$ most of the imposed current flows through the second IS (from the left side), similar to the results of Figure 10 (where $p = 0.1$) for $T_L = 1.5\mathrm{K}$, and of Figure 20 for $T_L = 4\mathrm{K}$ and $p = 0$. For stronger imposed current, $I \geq 0.3\,\mu\mathrm{A}$, most of the current flows, to similar amounts, through this and the next but one IS to the right (in which the intrinsic current has the same direction). Such splitting of the increasing ASDC into essentially two parts has also been found in figures 8 and 10 of [40], in both cases for $T_L = 1.5\mathrm{K}$.

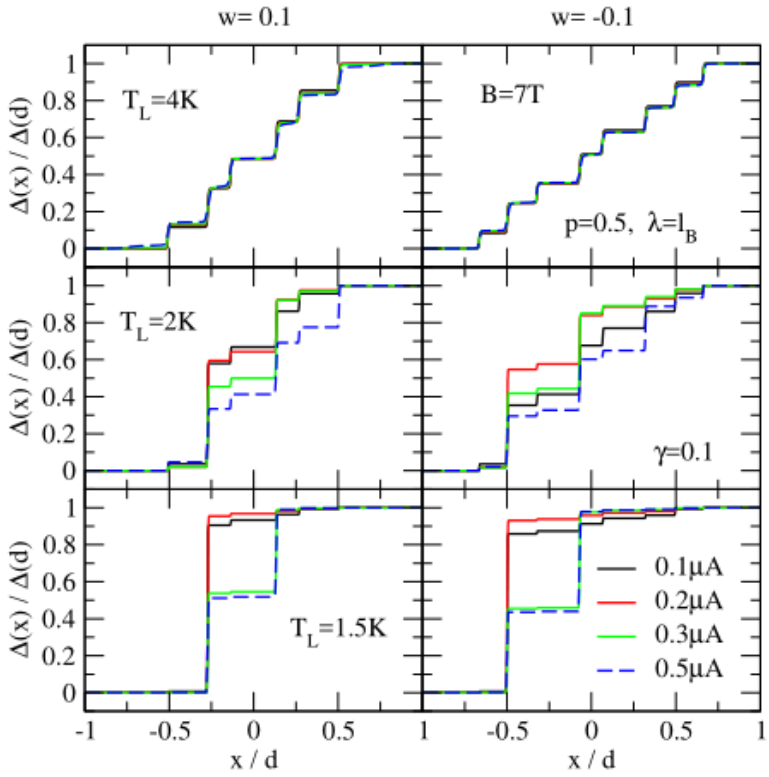


**Figure 21** Normalized Hall potential as in Figure 20, but for Joule heating with $p = 0.5$, $B = 7\,\mathrm{T}$, and lattice temperatures $T_L$ as indicated.

It should be mentioned that the data of Figure 21 were obtained by a procedure, in which magnetic field and imposed current are introduced at high temperature, $T_L = 50\mathrm{K}$, and then the temperature is lowered stepwise, and in each step self-consistency of the effective potential, electrochemical potential, electron density, position-dependent conductivity tensor, current density and local electron temperature is obtained by iteration. For $B = 7\mathrm{T}$ and $I \leq 1.1\,\mu\mathrm{A}$, we

obtained convergence down to temperatures $T_L \leq 2\mathrm{K}$. An alternative procedure is to start with the equilibrium state with an applied magnetic field at low temperature, and then to increase the imposed current stepwise. Again self-consistency must be achieved at each step. For $B = 7\mathrm{T}$ and $T = 2\mathrm{K}$, this procedure converged for $I \leq 0.85\,\mu\mathrm{A}$.

### *4.6 B-dependence of the Current Distribution*

Since at low temperatures and for magnetic field values within the $(\nu = 2)$-QHP the current is carried by incompressible stripes, and since their position changes with $B$ (see Figure 5), we expect that the spatial distribution of the ASDC changes strongly with changing magnetic field $B$. A survey over the $B$-dependence of the current density is given in Figure 22. To keep things simple, not the current density is shown, but the normalized Hall potential $H(x;I) = [\mu^*(x) - \mu^*(-d)]/[\mu^*(d) - \mu^*(-d)]$, so that finite current density is indicated by finite slope of $H(x;I)$. Since $H(x;I)$ increases, for each value of $B$ and of $I$, from $H(-d;I) = 0$ to $H(d;I) = 1$, in Figure 22 results for neighboring $B$-values are shifted by one. Since in thermal equilibrium, $I = 0$, the models have inversion symmetry, $n_{\mathrm{el}}(-x) = n_{\mathrm{el}}(x)$, the current density in the linear response limit has the same symmetry, $j_y(-x) = j_y(x)$, and $H(x; I \to 0)$ increases at $-x$ by the same amount as at $x$. This symmetry is rapidly destroyed with increasing ASDC.

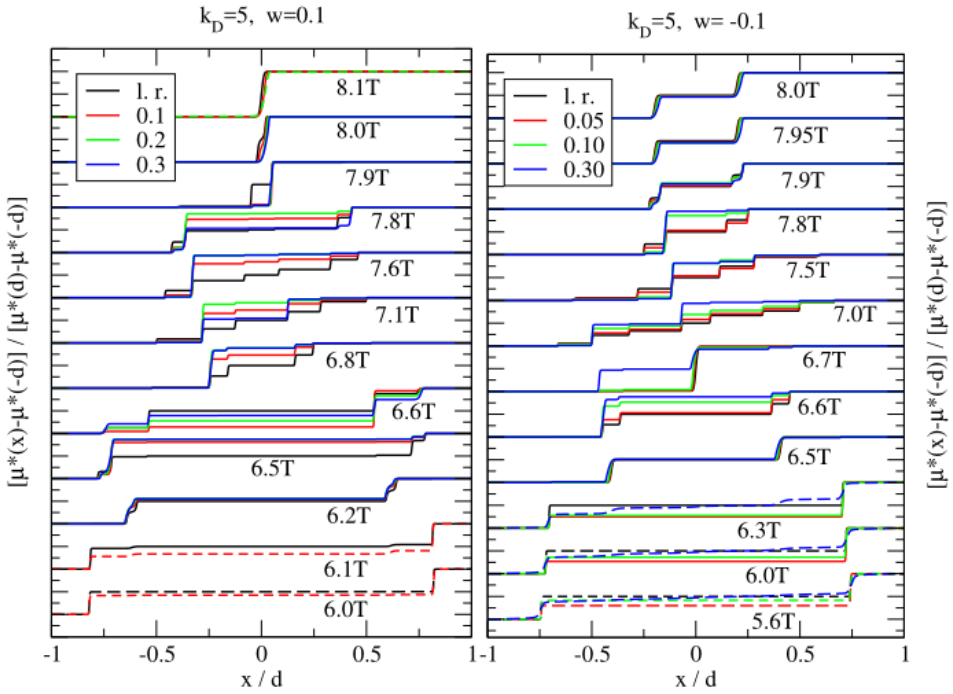


**Figure 22** Normalized Hall potentials for the two modulation models with $k_D = 5$: left panel for $w = 0.1$, right panel for $w = -0.1$. The colors indicate the linear response results (black) and the results for three finite values of $I$, given in $\mu$A. The results for adjacent $B$-values are vertically shifted by one; $T_L = 2\mathrm{K}$, $p = 0.5$, $\gamma = 0.1$, $\lambda = \ell_B$. Broken lines indicate states with poor quantization, $R_{\mathrm{long}} \gtrsim 10^{-4}\, h/e^2$.

Figure 22 shows, for lattice temperature $T_L = 2\mathrm{K}$ and the indicated values of the ASDC, how the normalized Hall potential $H(x;I)$ and thus the current distribution changes as the magnetic field sweeps through the $(\nu = 2)$-QHP. The left panel refers to the model of Figure 5 with $w = 0.1$, the

right panel refers to the model with $w = -0.1$. In order to obtain the data, first the equilibrium state at $T_L = 2\mathrm{K}$ and the required $B$-value are calculated, and then the ASDC is increased stepwise. Only relatively small ASDCs ($I \leq 3\mu\mathrm{A}$) are considered to avoid convergence problems. For the indicated $B$-values, calculations up to higher $I$-values are performed and the resulting resistance values are calculated. The results for $w = +0.1$ are shown in Figure 19. If we require as criterion for the IQHE $R_{\mathrm{long}} < 10^{-4} \cdot h/e^2$, in the left panel of Figure 22 this is satisfied for $I = 0.3\mu\mathrm{A}$ only in the interval $6.15\mathrm{T} \leq B \leq 8.0\mathrm{T}$. For $I = 0.3\mu\mathrm{A}$ and $B \leq 6.1\mathrm{T}$ and $B = 8.1\mathrm{T}$, this criterion is not satisfied and the corresponding results are indicated by broken lines. For the right panel, similar calculations show that the criterion for $I = 3.0\mu\mathrm{A}$ is not satisfied for $B \leq 6.3\mathrm{T}$. For $B = 5.6\mathrm{T}$, it is not satisfied for any value of $I$, but for $I = 0.1\mu\mathrm{A}$, it is satisfied for $B \geq 6.0\mathrm{T}$.

## 5. Summary and Discussion

In this article, a theory with numerical calculations is presented, which is able to explain many experimental results obtained on narrow Hall bars in the situation of the integer quantum Hall effect (IQHE) and its breakdown enforced by strong applied source-drain-currents (ASDCs). In order to simplify the calculations, a 2DES was considered in a Hall bar with translation-invariance in $y$-direction and lateral confinement in $x$-direction. Spin-splitting was neglected and the Coulomb interaction between electrons was considered in a Hartree-like approximation, neglecting exchange and correlation effects. We will comment on these approximations below.

### *5.1 Thermal Equilibrium*

The basic ingredient of the theory is the peculiar screening behavior of a 2DES in strong perpendicular magnetic fields at low temperatures, which is approximated by the interaction of an electron with the electrostatic field generated by the total density of the 2DES. If the spatial variation in the resulting screened confinement potential $U(x)$ is slow on the scale of the magnetic length $\ell_B$, this Hartree approximation can be simplified to the Thomas-Fermi approximation, in which the Landau quantization leads to a position-dependent energy-band-structure of the type $\varepsilon_n(x) = U(x) + \hbar\omega_c(n + 1/2)$. The corresponding thermodynamic density of states (TDOS) exhibits, at fixed position $x$, sharp maxima of the energy-dependence at the energy-eigenvalues $\varepsilon_n(x)$ and it is very small in-between these values. Its collision broadening should be calculated consistently with the conductivity tensor, e.g., in the self-consistent Born approximation [29, 34] or the simpler Gaussian approximation [37] considered here.

If the average electron density is fixed and sufficiently large, self-consistent calculation of electron density $n_{el}(x)$ and screened confinement potential $U(x)$ leads to alternating *compressible* and *incompressible* stripes. In the *compressible* stripes, one of the energy bands is "pinned" to the spatially constant electrochemical potential $\mu^*$ ($|\varepsilon_n(x) - \mu^*| \lesssim k_B T$), so that at sufficiently low temperatures (and small collision broadening) the band energy $\varepsilon_n(x)$ is nearly constant, whereas the electron density varies (compare Figure 3). In the *incompressible* stripes (ISs), located between two compressible stripes, in which neighboring Landau bands are pinned to $\mu^*$, the electron density $n_{el}(x)$ is spatially constant, because a fixed number of Landau bands with energies $\varepsilon_n(x) < \mu^*$ is occupied [25, 26]. The number of ISs, which can develop at sufficiently low temperatures, depends on the magnetic field and on the confinement potential, which in the

present context are determined by the position-dependence of the donor density. Figure 6 shows an example with six ISs.

### *5.2 Stationary, Dissipative Currents*

To describe the response of such a system to an ASDC, two basic assumptions were made. The first assumption is that a *stationary non-equilibrium state* carrying an imposed, dissipative current, can be treated as a state in *local equilibrium*, i.e. with position-dependent thermodynamic quantities, like energy eigenvalues, temperature, and electrochemical potential, which satisfy locally the same thermodynamic relations as in thermodynamic equilibrium. The second assumption is *a local, linear relation* (Ohm's law) between the density $\mathbf{j}(\mathbf{r}) = \hat{\sigma}(\mathbf{r})\mathbf{E}(\mathbf{r})$ of the ASDC and the gradient of the electrochemical potential, $\mathbf{E}(\mathbf{r}) = \nabla\mu^*(\mathbf{r})/e$, as "driving electric field". The position-dependent conductivity tensor $\hat{\sigma}(\mathbf{r})$ should depend on the local thermodynamic variables in just the same way as it would in a homogeneous equilibrium system. The desired solution should satisfy both assumptions self-consistently. Since an ASDC generates a finite current density in the sample, this leads to a position-dependent electrochemical potential and, as a consequence, to a dependence of electron density, confinement potential, and conductivity tensor on the ASDC. Because of Joule heating, also a position-dependent increase in the electron temperature $T_{el}(\mathbf{r})$ over the constant lattice temperature $T_L$ has to be expected.

If the ASDC is not too large, one may neglect the heating effect and put in the considered stripe geometry $T_{el}(x) \equiv T_L$. The calculations with this approximation [28, 29, 33] could already explain the physical basis of many of the experimental results [12]. They showed, firstly, that at sufficiently low temperatures in certain magnetic field intervals, i.e., the quantum Hall plateaus (QHPs), incompressible stripes exist, in which the filling factor assumes an integer value, $\nu(x) = n$, and in which longitudinal and Hall resistivity assume the quantized free-electron values, because in the ISs no quasi-elastic scattering and, therefore, no dissipation is possible. Secondly, they showed that, with decreasing temperature, the ASDC becomes increasingly confined to these developing ISs (as is also shown in Figures 9 and 10), thereby minimizing the entropy production, so that the quantization of the global resistances, $R_{\mathrm{long}} = 0$ and $R_{\mathrm{Hall}} = h/(ne^2)$, is approached with exponentially small deviations. Thus, the dissipation-less current in the IQHE is carried by states far below the local value of the electrochemical potential.

As discussed previously [27], confinement of the applied current to incompressible stripes, which occupy only a small fraction of the sample width, can explain several astonishing experimental observations, which we will not discuss in detail, e.g., the frequency of magnetoplasmons in special, narrow Hall bars [48], or the avalanche-like position-dependence of the breakdown of the IQHE in Hall bars, into which a supercritical current is injected [22-24], or the breakdown of the IQHE caused by quasi-elastic inter-Landau-level scattering (QUILLS) [47], mentioned earlier.

Joule heating becomes more important if the ASDC becomes larger. One example is the current-induced asymmetry of the spatial distribution of the ASDC. With increasing current strength, the ISs, in which the intrinsic Hall-current has the same direction as the ASDC, become wider and contribute more to the total current than the ISs, in which the intrinsic current has the opposite direction. This asymmetry effect, which becomes more effective with decreasing temperature (see Figures 9, 10 and 11), has been observed [11] and investigated [39]

experimentally, and first calculated [28] and explained [38] without considering Joule heating. However, at larger currents, when Joule heating becomes more important, it may reduce the asymmetry and, eventually, lead to the breakdown of the IQHE (see Figures 12, 13 and 20) [43].

The current-induced, continuous breakdown of the IQHE, calculated for the low-$B$ part of the ($\nu = 2$)-QHP, where only ISs near the sample edge exist ("edge-dominated" region), is in good qualitative agreement with the experimental finding: for larger $B$ the breakdown happens at a larger critical current $I_{cr}(B)$, and in the resistive regime $I > I_{cr}(B)$ the derivative of the function $R_{\mathrm{long}}(I)$ decreases with increasing $B$ (see Figures 17, 18 and 19 and figure 3 of of the experimental study [39]). For the high-$B$ region of this QHP the situation is different. Experimentally, one finds under the conditions of the IQHE, a current distribution over a wide part of the sample ("bulk-dominated" region) and a critical current $I_{cr}(B)$, which decreases with increasing $B$. In the resistive regime $I > I_{cr}(B)$, the derivatives of the measured $R_{\mathrm{long}}(I)$-curves increase with increasing $B$ and are much larger than the corresponding slopes in the edge-dominated regime. The corresponding calculations for samples with homogeneous donor charge did not converge (Figure 17). The calculation for a modulated donor charge-density, which leads to a $n_{el}(x)$ with two maxima and a minimum in the center, yields also a critical $I_{cr}(B)$, which decreases with increasing $B$ but with much smaller derivatives of the $R_{\mathrm{long}}(I)$-curves than in the low-$B$ part of the QHP (see Figure 18). Other modulations of donor and electron density, which were considered to simulate a bulk-dominated behavior, could also not reproduce the experimental findings (see Figure 19). However, it seems that the details of the current-induced breakdown of the IQHE in the "bulk-dominated" regime depend strongly on the spatial variations of the electron density in the region near its maxima.

### *5.3 Some Final Remarks*

In order to keep the calculations manageable and approximations reliable, we considered a 2DES with translation-invariance in one direction. This makes, of course, a quantitative agreement of the calculated results with experiments on a Hall bar with source and drain contacts practically impossible, but may yield a reasonable approximation of the behavior of a long sample far from these contacts. Due to the lateral confinement, the electron density in the Hall bar will change with position, and in different parts of the sample, a different number of Landau levels will be occupied. If, in a homogeneous perpendicular magnetic field, somewhere in the sample several Landau levels are occupied and the collision broadening of the Landau levels is not too large, the peculiar screening properties of the system at low temperatures will separate the sample into compressible regions, in which a single Landau level is pinned to the electrochemical potential, and incompressible regions between two neighboring compressible regions, in which adjacent energy levels are pinned. Of course, in real Hall bars, strong magnetic fields lead to spin-splitting of the Landau energies. It is well known that, in GaAs(AlGa)As-heterostructures, the electron-exchange interaction leads to a large exchange-enhancement of the spin-splitting [34]. In a naive Hartree-Fock approximation, the obtained spin-splitting is unrealistically large [34] and the Hartree-type screening is partly destroyed [35]. To get reasonable results for spin splitting and screening, a much more ambitious treatment of the many-body Coulomb interaction, e.g., the self-consistent Hartree-Fock approximation, is necessary [34]. This will also lead to similar screening results as the Thomas-Fermi approximation [36]; however, with compressible stripes, in

which Landau energies with the same spin-direction are pinned to the electrochemical potential, and ISs, which are spin-polarized if their integer filling factor $\nu(x) = n$ is odd, and not spin-polarized if $n$ is even.

The experimental results in the bulk-dominated regime indicate spatial fluctuations of the electron density near its maxima, perhaps generated by fluctuations of the donor distribution generating the confinement potential. These fluctuations certainly destroy the translation-invariance but will give rise to a structure of alternating compressible and incompressible regions. In the compressible regions, the current-driving electric field is totally screened, whereas in the incompressible regions dissipation-less Hall currents can flow. In order to understand the IQHE, one needs to assume an incompressible region between current source and drain, which transports the total ASDC and has everywhere the same integer value of the local filling factor. This incompressible region may be connected, perhaps with enclosed compressible islands, or disconnected like parallel ISs.

An interesting aspect of the presented theory is that it is very plausible for the dissipative high-temperature regime, where it essentially reproduces the well-known Drude results, and that it needs no other modification as a reasonable treatment of screening effects to explain the IQHE. There is no localization assumptions or similar hypothesis required.

There remain, of course, some interesting questions. Is it possible to repeat the calculations in the self-consistent Hartree-Fock approximation? Some results based on a local parameterization of the exchange potential have been published [49, 50]. Can one do similar calculations for a rectangular sample with source and drain contacts? What are the consequences of screening effects for the fractional QHE?

There are also some questions, which arise from the calculations. For a sufficiently large ASDC, the calculated temperature-dependence of the longitudinal resistance shows discontinuities, indicating hysteretic discontinuous transitions between resistive “high-temperature” states and states showing the IQHE (Figures 15 and 16). Is it possible to verify this situation experimentally? Usually the scanning-force-microscope experiments are carried out at fixed temperature. Perhaps one can find interesting behavior as a function of the current strength, while keeping the magnetic field and (sufficiently low) temperature fixed. This would probably require to measure longitudinal and Hall resistance very precisely.

## Appendix A. Mathematical Details

The model assumptions of metal plates in the halfplanes $z = 0$ and $|x| > d$ and of a charge density $\rho(x)\delta(z)$ in the stripe $-d < x < d$ allow to express the electrostatic potential $V(x,z)$, which has to satisfy, in regions without charges, the Laplace equation, in terms of this charge density and the constant potential values $V(x,0) = V_L$ and $V(x,0) = V_R$ on the metal gates at $x < d$ and $x > d$, respectively. To this end, $V(x,z) = \mathrm{Im}F(\zeta)$ is written for $z \neq 0$ as imaginary part of a holomorphic function of $\zeta = x + iz$, which automatically satisfies the Laplace equation. To satisfy the boundary conditions for $z = 0$, one writes the potential $V(x,z) = V_G(x,z) + V_C(x,z)$ as the sum of two term, where $V_G(x,z) = \mathrm{Im}F_G(\zeta)$, with

$$F_G(\zeta) = iV_R + \frac{V_L - V_R}{\pi} \ln\{\frac{\zeta}{d} - \sqrt{\zeta^2/d^2 - 1}\}, \quad (27)$$

is determined by the constant values $V_G(x,0) = V_L$ and $V_G(x,0) = V_R$ on the metal gates at $x < d$ and $x > d$, respectively, and $V_C(x,z)$ is determined by the charge densities in the stripe $z = 0$, $|x| < d$.

Since $\partial V/\partial x = \mathrm{Im} dF/d(\zeta)$ and $\partial V/\partial z = \mathrm{Re} dF/d(\zeta)$, and the derivative $F_G{}'(x + i0)$ is purely imaginary for $|x| < d$, $V_G$ is not affected by the requirement of electrostatics, that for $|x| < d$

$$\kappa_> \frac{\partial V}{\partial z}(x, z = 0^+) - \kappa_< \frac{\partial V}{\partial z}(x, z = -0^+) = -4\pi\rho(x) \quad (28)$$

must hold, where $\kappa_>$ and $\kappa_<$ are the dielectric constants of the half-spaces $z > 0$ and $z < 0$, respectively. Anticipating $\frac{\partial V}{\partial z}(x, z = -0^+) = -\frac{\partial V}{\partial z}(x, z = 0^+)$ and defining $r(x) = -4\pi\rho(x)/(\kappa_> + \kappa_<)$, the potential generated by the charge density in the stripe, $V_C(x,z) = \mathrm{Im} F_C(\zeta)$, is obtained from a holomorphic function satisfying

$$\mathrm{Re}\frac{dF_C}{d\zeta}(x + i0^+) = r(x) \text{ if } |x| < d, \ \mathrm{Im}\frac{dF_C}{d\zeta}(x + i0^+) = 0 \text{ if } |x| > d \quad (29)$$

These requirements are satisfied by [26, 28]

$$\frac{dF_C}{d\zeta}(\zeta) = \frac{i}{\pi\sqrt{d^2 - \zeta^2}} \int_{-d}^{d} dt \frac{\sqrt{d^2 - t^2}}{\zeta - t} r(t). \quad (30)$$

If $r(t)$ in Eq.(30) is replaced by a constant $r_0$, the $t$-integral can be carried out analytically, with the result $F'_C(\zeta) = r_0(1 + i\zeta/\sqrt{d^2 - \zeta^2})$. As a consequence, a constant donor density $n_D(x) \equiv n_0$ in the stripe $z = 0$, $|x| < d$ generates an electrostatic potential $V_D(x, 0^+) = -r_0\sqrt{d^2 - x^2}$ in $|x| < d$ and $V_D(x, 0^+) = 0$ for $|x| > d$ (up to an irrelevant constant, which is taken to vanish). With $\overline{\kappa} = (\kappa_> + \kappa_<)/2$ and $r_0 = -2\pi e n_0/\overline{\kappa}$, this leads to the donor-produced potential energy

$$U_D(x) = -eV_D(x) = -E_0\sqrt{1 - x^2/d^2}, \quad E_0 = 2\pi e^2 n_0 d/\overline{\kappa}, \quad (31)$$

of an electron in the stripe [26, 28]. If $n_D(x)$ is not constant, $V_D(x)$ must be calculated numerically. In the stripe $|x| < d$ the potential $V_C(x, 0^+) = \mathrm{Im} F_C(x + i0^+)$ can be calculated from Eq.(30) as

$$V_C(x) = -\frac{1}{\pi}\int_{-d}^{d} dt \ K(x,t)\, r(t), \quad (32)$$

with the kernel

$$K(x,t) = \ln \left| \frac{\sqrt{(d^2 - x^2)(d^2 - t^2)} + d^2 - tx}{(x - t)d} \right| \quad (33)$$

With $r(x) = -(2\pi e/\overline{\kappa})[n_D(x) - n_{el}(x)]$ equations (32) and (33) allow to calculate the electrostatic potential created by the charge densities of donors and electrons. On the other hand, the position dependence of the electron density in thermal equilibrium is determined by the effective electrostatic potential. Thus we have to calculate $n_{el}(x)$ and $V_C(x)$ self-consistently.

The presence of the metal gates requires, according to Eq.(29), $\mathrm{Im} F'(x + i0) = \partial V(x,0)/\partial x = 0$ if $|x| > d$, that the potential created by the charges in the Hall bar is constant on the metal plates. On the other hand, this potential induces charge densities $\rho_{ind}(x)$ on the metal plates, according to

$$\frac{\partial V_C}{\partial Z}(x, 0^+) = \mathrm{Re}\frac{dF_C}{d\zeta}(x + i0^+) = -\frac{2\pi}{\overline{\kappa}}\rho_{ind}(x) \text{ for } |x| > d. \quad (34)$$

The total induced charge on the right gate, $Q_R = \int_d^\infty dx\, \rho_{ind}(x)$, follows from Eq.(30), with $1/\sqrt{d^2 - (x + i0^+)^2} = i/\sqrt{x^2 - d^2}$, as

$$Q_R = -\int_d^\infty dx \frac{1}{\pi}\int_{-d}^{d} dt \frac{\sqrt{d^2 - t^2}}{(x - t)\sqrt{x^2 - d^2}} \rho(t)$$

$$= -\frac{1}{\pi}\int_{-d}^{d} dt \ \rho(t)\left(\frac{\pi}{2} + \arcsin\frac{t}{d}\right) = -\frac{2}{\pi}\int_{-d}^{d} dt \ \rho(t) \arctan\sqrt{\frac{d + t}{d - t}}. \quad (35)$$

The corresponding result $Q_L$ for the left gate is obtained from Eq.(35) by replacing $t$ by $-t$ in the arguments of the arcsin and of the square root. Thus, the sum of the induced charges, $Q_L + Q_R = -\int_{-d}^{d} dx\rho\,(x)$, compensates the free charges, and their difference vanishes, if the charge density in the Hall bar is symmetric, $\rho(-x) = \rho(x)$ [28].

**Acknowledgments**

I am grateful to my former coworkers Kaan Güven and Afif Siddiki, who helped to develop this self-consistent theory of screening and magneto-transport and produced many encouraging results. I am also indebted to my experimental colleague Jürgen Weis and his group, especially Kosta Panos, for a fruitful cooperation and many useful hints to generalize and improve the theory. I want to thank Klaus von Klitzing for his interest in the progress of this work and for the possibility to perform this work using the equipment of the Max-Planck-Institute for Solid-State-Research. My special thanks go to Janos Hajdu for a critical reading of the manuscript and for many valuable suggestions to improve it.

**Author Contributions**

Rolf R. Gerhardts did all work.

**Competing Interests**

The authors have declared that no competing interests exist.

**References**

1. von Klitzing K, Dorda G, Pepper M. New method for high-accuracy determination of the fine-structure constant based on quantized Hall resistance. Phys Rev Lett. 1980; 45: 494.
2. Bachmair H, Göbel EO, Hein G, Melcher J, Schumacher B, Schurr J, et al. The von Klitzing resistance standard. Physica E. 2003; 20: 14.
3. Göbel EO, Siegner U. The New International System of Units (SI). Wiley-VCH. Berlin. 2019.
4. Tsui DC, Störmer HL, Gossard AC. Two-dimensional magnetotransport in the extreme quantum limit. Phys Rev Lett. 1982; 48: 1559
5. Prange RE, Girvin SM. The quantum Hall effect. Springer-Verlag: New York. 1987.
6. Janßen M, Viehweger O, Fastenrath U, Hajdu J. Introduction to the theory of the integer quantum Hall effect. Weinheim (Germany): VCH Verlagsgesellschaft mbH; 1994.
7. Datta S. Electronic transport in mesoscopic systems. Cambridge University Press. 1995.
8. Ezawa ZF. Quantum Hall effects. Field theoretical approach and related topics. 2nd ed. Singapore: World Scientific; 2008. pp730.
9. von Klitzing K. The quantum Hall effect - an edge phenomenon? Physica B. 1993; 184: 1-6.
10. Weitz P, Ahlswede E, Weis J, von Klitzing K, Eberl K. A low-temperature scanning force microscope for investigating buried two-dimensional electron systems under quantum Hall conditions. Appl Surf Sci. 2000; 157: 349.
11. Weitz P, Ahlswede E, Weis J, von Klitzing K, Eberl K. Hall-potential investigations under quantum Hall conditions using scanning force microscopy. Physica E. 2000; 6: 247

12. Ahlswede E, Weitz P, Weis J, von Klitzing K, Eberl K. Hall potential profiles in the quantum Hall regime measured by a scanning force microscope. Physica B. 2001; 298: 562.
13. Ahlswede E, Weis J, von Klitzing K, Eberl K. Hall potential distribution in the quantum Hall regime in the vicinity of a potential probe contact. Physica E. 2002; 12: 165.
14. Chklovskii DB, Shklovskii BI, Glazman LI. Electrostatics of edge channels. Phys Rev B. 1992; 46: 4026.
15. Chklovskii DB, Matveev KA, Shklovskii BI. Ballistic conductance of interacting electrons in the quantum Hall regime. Phys Rev B. 1993; 47: 12605.
16. Wulf U, Gudmundsson V, Gerhardts RR. Screening properties of the two-dimensional electron gas in the quantum Hall regime. Phys Rev B. 1988; 38: 4218.
17. Gudmundsson V, Gerhardts RR. Interpretation of experiments implying density of states between landau levels of a two-dimensional electron gas by a statistical model for inhomogeneities. Phys Rev B. 1987; 35: 8005.
18. Efros AL. Non-linear screening and the background density of 2DEG states in magnetic field. Solid State Commun. 1988; 67: 1019.
19. Efros AL. Homogeneous and inhomogeneous states of a two-dimensional electron liquid in a strong magnetic field. Phys Rev B. 1992; 45: 11354.
20. Efros AL, Pikus FG, Burnett VG. Density of states of a two-dimensional electron gas in a long-range random potential. Phys Rev B. 1993; 47: 2233.
21. Güven K, Gerhardts RR, Kaya II, Sagol BE, Nachtwei G. Two-level model for the generation and relaxation of hot electrons near the breakdown of the quantum Hall effect. Phys Rev B. 2002; 65: 155316.
22. Kaya II, Nachtwei G, von Klitzing K, Eberl K. Spatially resolved monitoring of the evolution of the breakdown of the quantum Hall effect: Direct observation of inter-Landau-level tunneling. Europhys Lett. 1999; 46: 62.
23. Kaya II, Nachtwei G, von Klitzing K, Eberl K. Spatial evolution of hot-electron relaxation in quantum Hall conductors. Phys Rev B. 1998; 58: R7536.
24. Kaya II, Nachtwei G, Sagol BE, von Klitzing K, Eberl K. Spatial evolution of the generation and relaxation of excited carriers near the breakdown of the quantum Hall effect. Physica E. 2000; 6: 128.
25. Lier K, Gerhardts RR. Self-consistent calculations of edge channels in laterally confined two-dimensional electron systems. Phys Rev B. 1994; 50: 7757.
26. Oh JH, Gerhardts RR. Self-consistent Thomas-Fermi calculation of potential and current distributions in a two-dimensional Hall bar geometry. Phys Rev B. 1997; 56: 13519.
27. Gerhardts RR. The effect of screening on current distribution and conductance quantisation in narrow quantum Hall systems. Phys Status Solidi B. 2008; 245: 378.
28. Güven K, Gerhardts RR. Self-consistent local equilibrium model for density profile and distribution of dissipative currents in a Hall bar under strong magnetic fields. Phys Rev B. 2003; 67: 115327.
29. Siddiki A, Gerhardts RR. Incompressible strips in dissipative Hall bars as origin of quantized Hall plateaus. Phys Rev B. 2004; 70: 195335.
30. von Klitzing K, Gerhardts R, Weis J. 25 years of the quantum Hall effect. Physik J. 2005; 4: 37.

31. Gerhardts RR, Weis J, von Klitzing K. Quantum Hall Effect. In: Greenberger D, Hentschel K, Weinert F (editors) Compendium of Quantum Physics. Heidelberg: Springer; 2009. pp. 572-591.
32. Weis J, Gerhardts RR. Quantum Hall Effect. In: Saleem Hashmi (editor-in-chief) Reference Module in Materials Science and Materials Engineering. Oxford: Elsevier. 2016. pp. 1-13.
33. Siddiki A, Gerhardts RR. The interrelation between incompressible strips and quantized Hall plateaus. Int J Mod Phys B. 2004; 18: 3541.
34. Ando T, Fowler AB, Stern F. Electronic properties of two-dimensional systems. Rev Mod Phys. 1982; 54: 437.
35. Manolescu A, Gerhardts RR. Exchange-enhanced spin splitting in a two-dimensional electron system with lateral modulation. Phys Rev B. 1995; 51: 1703.
36. Manolescu A, Gerhardts RR. Coulomb effects on the quantum transport of a two-dimensional electron system in periodic electric and magnetic fields. Phys Rev B. 1997; 56: 9707.
37. Gerhardts RR. Path-integral approach to the two-dimensional magneto-conductivity problem. Z Physik B. 1975; 21: 285.
38. Gerhardts RR, Panos K, Weis J. Current-induced asymmetries of incompressible strips in narrow quantum Hall systems. New J Phys. 2013; 15: 073034.
39. Panos K, Gerhardts RR, Weis J, von Klitzing K. Current distribution and Hall potential landscape towards breakdown of the quantum Hall effect: A scanning force microscopy investigation. New J Phys. 2014; 16: 113071.
40. Gerhardts RR. Current distribution in narrow translation-invariant quantum-Hall-systems with lateral density modulation. New J Phys. 2019; 21: 073007.
41. Pfannkuche D, Hajdu J. Potential and current distribution in an ideal Hall bar. Phys Rev B. 1992; 46: 7032.
42. Keiter H. Über den Einfluß der Coulomb-Wechselwirkung zwischen den Elektronen auf den Restwiderstand im Magnetfeld. Z Physik. 1967; 198: 215.
43. Gerhardts RR. Effect of Joule heating on current-induced asymmetries and breakdown of the quantum Hall effect in narrow Hall bars. Physica E. 2017; 85: 38.
44. Kanamaru S, Suzuura H, Akera H. Spatial distributions of electron temperature in quantum Hall systems with compressible and incompressible strips. J Phys Soc Jpn. 2006; 75: 064701.
45. Panos K. Current distribution and Hall potential landscape within the quantum Hall effect in graphene and towards the breakdown in a (Al, Ga) As heterostructure. Thesis Universität Stuttgart. 2014.
46. Data of Figure 20 were shown in figure 10 of Ref.39 for another choice of coordinates
47. Eaves L, Sheard FW. Size-dependent quantised breakdown of the dissipationless quantum Hall effect in narrow channels. Semicond Sci Technol. 1986; 1: 346.
48. Holland S, Heyn C, Heitmann D, Batke E, Hey R, Friedland KJ, et al. Quantized dispersion of two-dimensional magnetoplasmons detected by photoconductivity spectroscopy. Phys Rev Lett. 2004; 93: 186804.
49. Bilgec G, Toffoli HÜ, Siddiki A, Sokmen I. The self-consistent calculation of exchange enhanced odd integer quantized Hall plateaus within Thomas–Fermi–Dirac approximation. Physica E. 2010; 42: 1058.
50. Akyüz GB, Siddiki A, Sökmen I. Magnetotransport calculations for two-dimensional electrons with exchange and correlation interactions. Physica E. 2015; 69: 364.


Enjoy *Recent Progress in Materials* by:

1. Submitting a manuscript
2. Joining in volunteer reviewer bank
3. Joining Editorial Board
4. Guest editing a special issue

For more details, please visit:
http://www.lidsen.com/journals/rpm